

## Article

# Photo-Oxidation of Glycerol Catalyzed by Cu/TiO<sub>2</sub>

Osmin Avilés-García <sup>1</sup>, Arisbeht Mendoza-Zepeda <sup>1</sup>, Alejandro Regalado-Méndez <sup>2</sup> , Jaime Espino-Valencia <sup>3</sup>, Sandra L. Martínez-Vargas <sup>1</sup>, Rubi Romero <sup>1</sup> and Reyna Natividad <sup>1,\*</sup> 

<sup>1</sup> Chemical Engineering Laboratory, Centro Conjunto de Investigación en Química Sustentable, UAEM-UNAM, Universidad Autónoma del Estado de México, km 14.5 Toluca-Atlacomulco Road, Toluca 50200, Mexico, Mexico; agosmin@gmail.com (O.A.-G.); ary.zepeda@hotmail.com (A.M.-Z.); sandraluz\_mtzv@hotmail.com (S.L.M.-V.); romeror@uaemex.mx (R.R.)

<sup>2</sup> Research Laboratories, Campus Puerto Ángel, Universidad del Mar, Puerto Ángel 70902, Oaxaca, Mexico; alejandro.regalado33@gmail.com

<sup>3</sup> Chemical Engineering Faculty, Universidad Michoacana de San Nicolás de Hidalgo, Edif. V1, Ciudad Universitaria, Morelia 58060, Michoacán, Mexico; jespino@umich.mx

\* Correspondence: rnatividadr@uaemex.mx; Tel.: +52-722-2766610 (ext. 7723)

**Abstract:** In the present study, glycerol was oxidized by photocatalysis to glyceraldehyde, formaldehyde, and formic acid. Copper-doped TiO<sub>2</sub> was synthesized by the evaporation-induced self-assembly approach and it was used as catalyst during the glycerol photo-oxidation reactions. The prepared mesoporous material exhibited high specific surface area (242 m<sup>2</sup>/g) and band gap energy reduction of 2.55 eV compared to pure titania (3.2 eV) by the synthesis method due to the presence of copper cations (Cu<sup>2+</sup> identified by XPS). The catalyst showed only anatase crystalline phase with nanocrystals around 8 nm and irregular agglomerates below 100 μm. The selectivity and formation rate of the products were favored towards formaldehyde and glyceraldehyde. The variables studied were catalyst amount, reaction temperature, and initial glycerol concentration. The response surface analysis was used to evaluate the effect of the variables on the product's concentration. The optimized conditions were 0.4 g/L catalyst, 0.1 mol/L glycerol, and temperature 313.15 K. The response values under optimal conditions were 3.23, 8.17, and 1.15 mM for glyceraldehyde, formaldehyde, and formic acid, respectively. A higher selectivity towards formaldehyde was observed when visible light was used as the radiation source. This study is useful to evaluate the best reaction conditions towards value-added products during the oxidation of glycerol by photocatalysis using Cu/TiO<sub>2</sub>.

**Keywords:** Cu/TiO<sub>2</sub>; photo-oxidation; glycerol; products; optimization



**Citation:** Avilés-García, O.; Mendoza-Zepeda, A.; Regalado-Méndez, A.; Espino-Valencia, J.; Martínez-Vargas, S.L.; Romero, R.; Natividad, R. Photo-Oxidation of Glycerol Catalyzed by Cu/TiO<sub>2</sub>. *Catalysts* **2022**, *12*, 835. <https://doi.org/10.3390/catal12080835>

Academic Editors: Detlef W. Bahnemann, Ewa Kowalska, Ioannis Konstantinou, Magdalena Janus, Vincenzo Vaiano, Wonyong Choi and Zhi Jiang

Received: 19 May 2022

Accepted: 27 July 2022

Published: 29 July 2022

**Publisher's Note:** MDPI stays neutral with regard to jurisdictional claims in published maps and institutional affiliations.



**Copyright:** © 2022 by the authors. Licensee MDPI, Basel, Switzerland. This article is an open access article distributed under the terms and conditions of the Creative Commons Attribution (CC BY) license (<https://creativecommons.org/licenses/by/4.0/>).

## 1. Introduction

Biodiesel is a widely used energy alternative because it is environmentally friendly compared to fossil fuels. However, the production of biodiesel generates a large amount of glycerol as the main waste byproduct in the triglyceride transesterification reaction [1], with an approximate formation weight ratio of 1:20 [2]. It is for this reason that interest in glycerol has increased towards its conversion into value-added products [3]. Selective oxidation of glycerol is a commonly used reaction for its conversion to chemicals of interest, such as dihydroxyacetone, glyceraldehyde, formaldehyde, and various acids (formic, glyceric, glycolic, oxalic, among others) [4,5].

Among the processes that have been carried out for the oxidation of glycerol are with heterogeneous [6] and homogeneous [7] catalysts, and microbial [8] and electrochemical [9] oxidation. Heterogeneous photocatalysis has been used as an alternative in the selective conversion of glycerol towards certain products of interest, because the reactions are performed under moderate conditions with relatively low energy consumption, using different types of solid catalysts such as ZnO, Bi<sub>2</sub>WO<sub>6</sub>, Pt/CNT, and TiO<sub>2</sub> [10–13]. Titanium dioxide is the most widely used semiconductor due to its excellent properties (low cost and toxicity, abundant, thermal, and chemical stability) [14,15]. The incorporation of metallic

and non-metallic species in TiO<sub>2</sub> in order to improve its photocatalytic performance has been approached by several investigations to extend its absorption spectrum and/or to reduce the recombination of the photogenerated electron/hole pairs [16,17]. Although most research has focused on the production of hydrogen from glycerol [18–20], the generation of products with industrial importance has been neglected. Furthermore, although photocatalysis is an advanced oxidation process, it can also be used to carry out partial oxidations of organic molecules towards certain compounds of interest. Table 1 summarizes the existing literature focused on the selective oxidation of glycerol by photocatalysis using pure TiO<sub>2</sub> and metal/TiO<sub>2</sub> as catalysts, the applied reaction conditions, and the relevant results regarding selectivity.

**Table 1.** Selective oxidation of glycerol by photocatalysis on TiO<sub>2</sub> and metal/TiO<sub>2</sub> catalysts.

Reaction Conditions	Studied Variables	Obtained Products	Selectivity (Principal Product)	Reference
Catalyst: Pt/TiO <sub>2</sub> Catalyst: 0.5 g/L Glycerol: 1 M Temperature: 30 °C Reactor type: batch λ: simulated sunlight Reaction time: 6 h	Catalyst synthesis method	Compound (selectivity): Glyceraldehyde (46%) Glycolaldehyde (54%)	Glycolaldehyde (54%)	[21]
Catalyst: Ag-AgBr/TiO <sub>2</sub> Catalyst: 1 g/L Glycerol: 4.5 mM Temperature: 25 °C Reactor type: batch λ: simulated sunlight Reaction time: 4 h	Catalyst type	Compound (selectivity): Glyceraldehyde (52%) Dihydroxyacetone (36%) Glycolic acid (8%) Glyceric acid (4%)	Glyceraldehyde (52%)	[22]
Catalyst: TiO <sub>2</sub> Catalyst: 3 g/L Glycerol: 0.3 M Temperature: 25 °C Reactor type: batch λ: 100–600 nm Reaction time: 24 h	Catalyst synthesis method	Compound (yield): Glycolaldehyde (39.2%) Glyceraldehyde (4.9%) Dihydroxyacetone (3.3%) Glycolic acid (2.2%) Hydroxypyruvic acid (2.1%) Formic acid (26.6%)	Glycolaldehyde (50%)	[23]
Catalyst: (Bi, Pd, Pt, Au)/TiO <sub>2</sub> Catalyst: 3 g/L Glycerol: 0.3 M Temperature: 25 °C Reactor type: batch λ: 200–600 nm Reaction time: 14 h	Metal type	Compound (yield): Glyceraldehyde (23.1%) Dihydroxyacetone (12%) Glycolic acid (10.7%) Hydroxypyruvic acid (13.6%) Formic acid (15.3%)	Glyceraldehyde (31%)	[24]
Catalyst: Au/TiO <sub>2</sub> Catalyst: 1 g/L Glycerol: 0.05 M Temperature: 90 °C Reactor type: batch (5 bar) λ > 420 nm Reaction time: 5 h	Support type	Glyceraldehyde Dihydroxyacetone Glycolic acid Oxalic acid	Dihydroxyacetone (63%)	[25]

Among the compounds obtained from the partial oxidation of glycerol (see Table 1), dihydroxyacetone, glyceraldehyde, glycolaldehyde, formaldehyde, and formic acid are considered chemicals with wide applications. Dihydroxyacetone is used as tanning compound in the cosmetics industry, as well as in the polymer industry as a monomer in the manufacture of biomaterials [26]. Glyceraldehyde is used in the skin care products industry [27]. Glycolaldehyde is the smallest molecule containing one hydroxyl group and one aldehyde group, which can be easily hydrogenated into value-added chemicals such as ethylene glycol under moderate reaction conditions [13]. Other expected products are formaldehyde and formic acid. Formaldehyde is widely used as a bactericide and a preservative of biological samples [28]. Formic acid is used in the leather industry and in agriculture [29]. Therefore, the generation of these compounds is of great industrial

importance. As observed in Table 1, the main obtained product and selectivity of the photocatalyzed glycerol oxidation varies according to type of catalyst, which also dictates the wavelength to conduct this reaction (100 to 600 nm).

In this work, TiO<sub>2</sub> doped with Cu cations was synthesized by the EISA (Evaporation-Induced Self-Assembly) method [30] and its photocatalytic performance was evaluated in the selective oxidation reaction of glycerol towards value-added products. Until now, no study using TiO<sub>2</sub> doped only with copper species and evaluated during the partial oxidation of glycerol has been reported [31,32]. Initial glycerol concentration, amount of catalyst, and temperature were the variables studied in order to obtain the best reaction conditions. The response surface methodology [33] was used to optimize the effect of the independent variables on the concentration of the products.

## 2. Results and Discussion

### 2.1. Characterization

The textural properties of the synthesized Cu/TiO<sub>2</sub> and TiO<sub>2</sub> catalysts are shown in Table 2. By nitrogen adsorption-desorption, it was observed that the incorporation of copper species into the TiO<sub>2</sub> structure increased the specific surface area and the pore volume with respect to the pure TiO<sub>2</sub> catalyst. The Cu/TiO<sub>2</sub> sample exhibited twice the surface area than that obtained with the pure TiO<sub>2</sub> material, and the pore volume increased from 0.26 to 0.48 cm<sup>3</sup>/g, which can be attributed to structural defects in the titania due to the presence of Cu cations [34]. The average pore diameter remained constant at 5.7 nm in both catalysts. High textural properties can promote better catalytic activity, since more organic molecules can be adsorbed [35].

**Table 2.** Textural properties and band-gap energies of Cu/TiO<sub>2</sub> and TiO<sub>2</sub> catalysts.

Catalyst	Specific Surface Area (m <sup>2</sup> /g)	Pore Volume (cm <sup>3</sup> /g)	Pore Diameter (nm)	Band Gap (eV)
Cu/TiO <sub>2</sub>	242.4	0.48	5.7	2.55
TiO <sub>2</sub>	121.5	0.26	5.7	3.24

Isotherms and pore size distributions of the synthesized materials are shown in Figure 1. The samples presented unimodal pore diameters with type IV isotherms and type H2 hysteresis cycles (relative pressure values between 0.5 and 0.9), which is characteristic of mesoporous materials forming a structure of interconnected pores [36]. The saturation point adsorption band for the Cu/TiO<sub>2</sub> sample is higher compared to that of the TiO<sub>2</sub> sample, which corresponds to a higher surface area, as can be seen in Figure 1a.

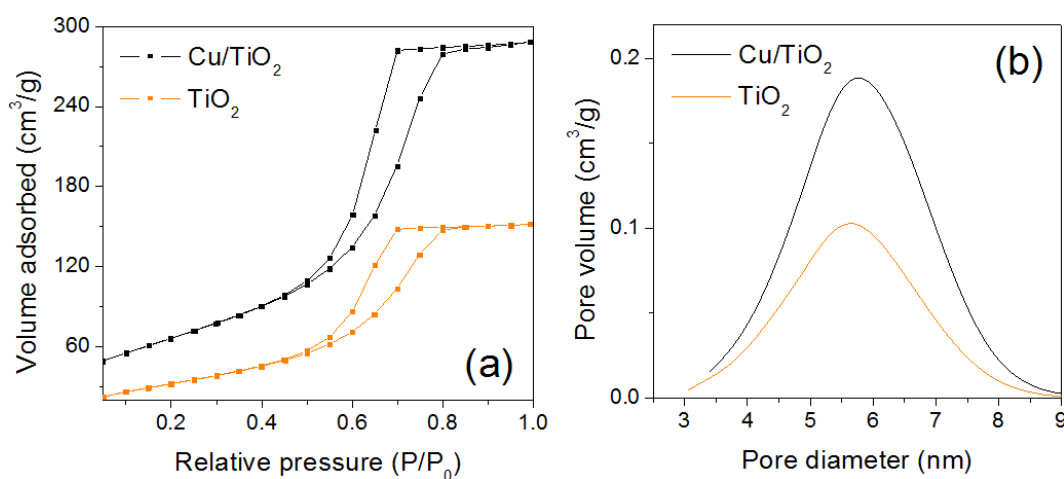


**Figure 1.** (a) N<sub>2</sub> adsorption-desorption isotherms and (b) pore size distributions of Cu/TiO<sub>2</sub> and TiO<sub>2</sub> catalysts.

Figure 2 shows the X-ray diffraction patterns of the synthesized catalysts. As can be seen, the materials exhibited only characteristic peaks of the anatase  $\text{TiO}_2$  crystalline phase corresponding to the planes (101), (004), (200), (105), (211), and (204), which are located at  $2\theta$  values of  $25.29^\circ$ ,  $37.94^\circ$ ,  $47.97^\circ$ ,  $53.91^\circ$ ,  $55.03^\circ$ , and  $62.65^\circ$ , respectively [37]. Copper species can be present in the  $\text{Cu}/\text{TiO}_2$  catalysts as  $\text{Cu}^{2+}$ , based on the used synthesis method [38], these species were later confirmed by XPS. These species exhibit ionic radii (0.072 nm) very similar to those of the  $\text{Ti}^{4+}$  species (0.068 nm) that are part of  $\text{TiO}_2$  and they are probably well dispersed within the structure of anatase crystals [39], so that no peak with respect to copper oxides was observed (see Figure 2). On the other hand, a slight shift in the position of the (101) anatase peak towards higher  $2\theta$  values is related to the crystal lattice distortion by Cu species, which reduces crystal growth [40]. As can be seen in Table 3, the addition of Cu cations in the titania reduces the average crystalline size from 8.22 nm to 7.98 nm, and an increase in the lattice distortion can be observed. The copper content in the catalyst, determined by atomic absorption spectroscopy, was 3.8 wt.%, as can be seen in Table 3. This value is in good agreement with the theoretical value of 3.9 wt.%. Energy dispersive spectroscopy analysis was also carried out and showed a value of 3.75 wt.% Cu (see Figure S1).

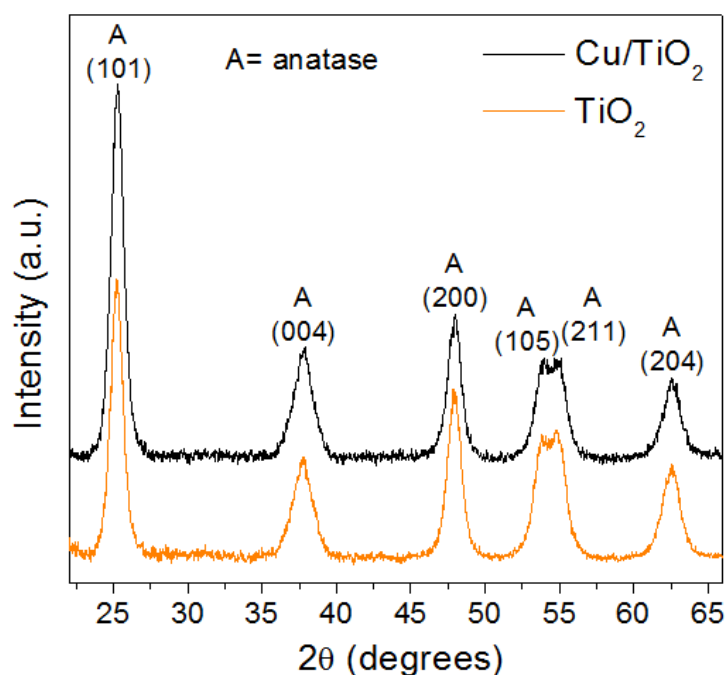


**Figure 2.** X-ray diffraction patterns of the synthesized  $\text{Cu}/\text{TiO}_2$  and  $\text{TiO}_2$  catalysts.

**Table 3.** Structural properties of  $\text{Cu}/\text{TiO}_2$  and  $\text{TiO}_2$  catalysts.

Catalyst	Anatase Plane (101)	Average Crystallite Size (nm)	Lattice Distortion (Å)	Cu wt.%
$\text{Cu}/\text{TiO}_2$	25.3	7.98	0.0198	3.8
$\text{TiO}_2$	25.2	8.22	0.0193	-

Images of catalysts  $\text{Cu}/\text{TiO}_2$  and  $\text{TiO}_2$  obtained by SEM are depicted in Figure 3. As can be seen, both materials exhibit particles with irregular shapes and sizes ranging from 30 to 100  $\mu\text{m}$ . This type of morphology is similar when compared to other investigations using the same synthesis methodology [41].

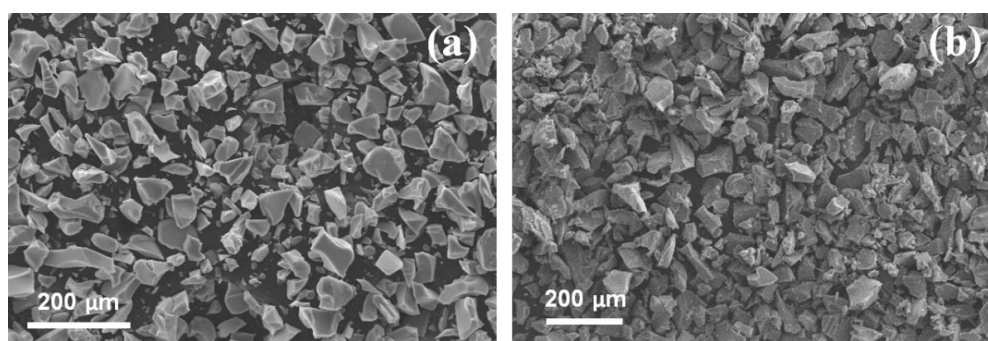


**Figure 3.** SEM images of catalysts (a) Cu/TiO<sub>2</sub> and (b) TiO<sub>2</sub>.

Transmission electron micrographs (TEM) and high-resolution transmission electron micrographs (HRTEM) for the synthesized catalysts are shown in Figure 4. Both materials, Cu/TiO<sub>2</sub> and TiO<sub>2</sub>, exhibit crystalline structures of irregular shapes and sizes between 7 and 10 nm, as can be seen in Figure 4a,c, which is in agreement with the XRD analyses during the estimation of the average anatase crystal size. HRTEM images shown in Figure 4b,d exhibit parallel lines that are related to the distance “d” between two planes (101) of anatase at a value of 0.35 nm [42], which is the preferential growth direction of the crystals. These images confirm the high crystallinity and well-defined structures of the catalysts.

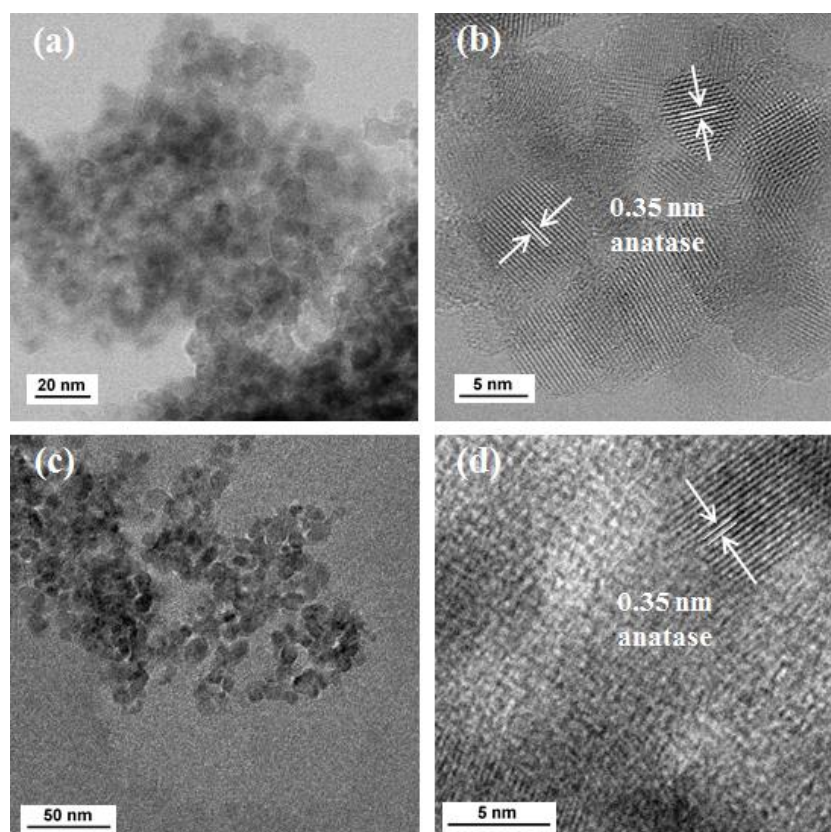


**Figure 4.** TEM and HRTEM micrographs of catalysts (a,b) Cu/TiO<sub>2</sub> and (c,d) TiO<sub>2</sub>.

The band-gap energies of the synthesized materials were determined by DRS analysis (see Table 2). The estimation of these values was carried out using the Kubelka–Munk function in Tauc graphs, as can be seen in Figure 5. The estimated value for the TiO<sub>2</sub> sample was 3.24 eV, which is in agreement with the reported band-gap value of anatase at 3.2 eV [43]. When copper is incorporated into TiO<sub>2</sub>, the band-gap value is reduced to 2.54 eV, which is related to charge transfers between the “3d” and “2p” orbitals of copper

and oxygen, respectively, just below the conduction band of the semiconductor [44]. The band-gap energy corresponds to the energy required to excite the semiconductor and thus be able to generate the electron/hole pairs responsible for the photocatalytic performance.

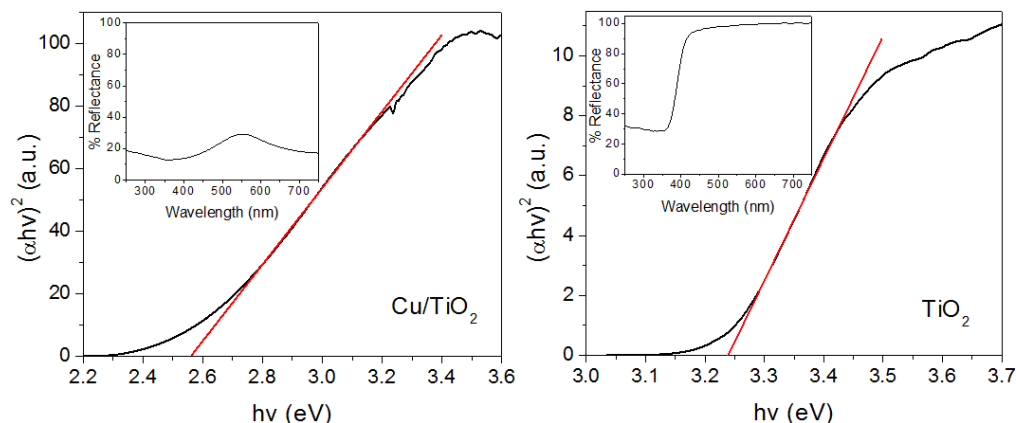


**Figure 5.** Tauc graphs for band-gap energies of synthesized catalysts. Inset: DRS spectra for each catalyst.

By means of X-ray photoelectron spectroscopy (XPS) analysis, the oxidation state of the species on the surface of the Cu/TiO<sub>2</sub> catalyst were established. Figure 6a shows the XPS spectra for Ti 2p with peaks for Ti 2p<sub>1/2</sub> and Ti 2p<sub>3/2</sub> at 264.2 eV and 258.6 eV, respectively, assigned to Ti<sup>4+</sup> [41]. Figure 6b shows the XPS spectra for O 1s with two contributions at 532.2 eV and 530.7 eV, assigned to surface oxygen (O-H) and oxygen into the TiO<sub>2</sub> lattice (O-Ti), respectively [45]. Figure 6c shows the XPS spectra for Cu 2p with two peaks at binding energies of 950 eV and 933 eV assigned to the Cu 2p<sub>1/2</sub> and Cu 2p<sub>3/2</sub> states, respectively, which correspond to Cu<sup>2+</sup> species forming Cu-O-Ti bonds [38].

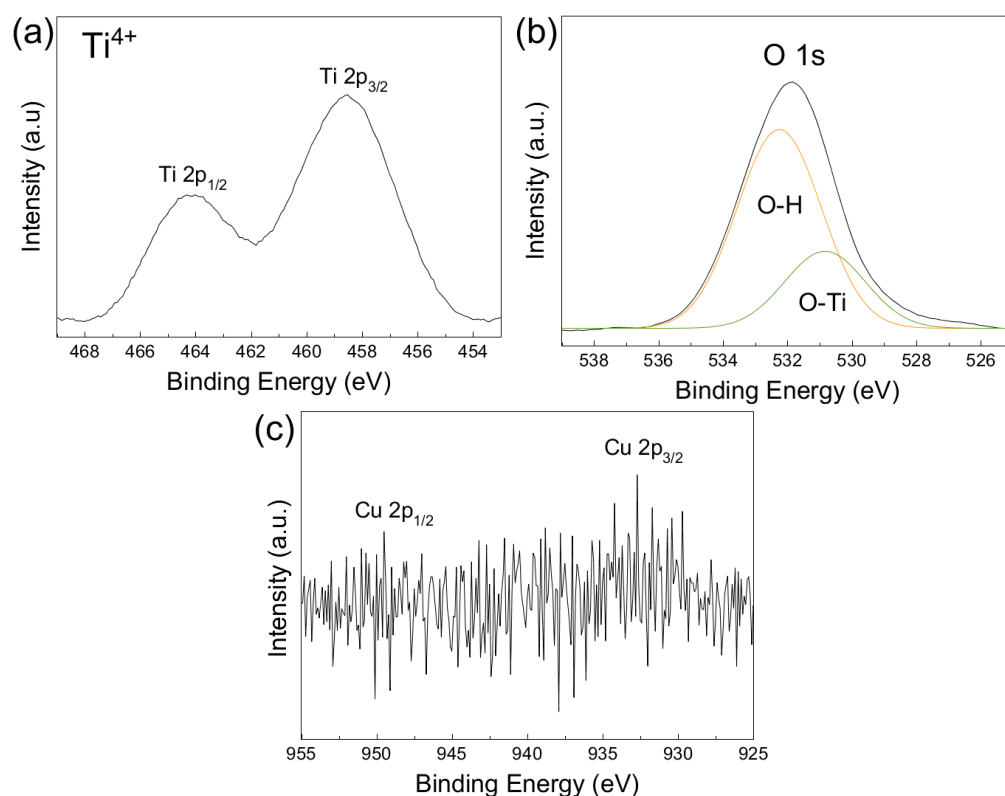


**Figure 6.** XPS spectra of (a) Ti 2p, (b) O 1s, and (c) Cu 2p for the Cu/TiO<sub>2</sub> catalyst.

## 2.2. Glycerol Photo-Oxidation

### 2.2.1. Effect of Catalyst Loading

The amounts of catalyst evaluated were selected based on the concentrations used for this type of photocatalytic reaction [21,46,47]. The glycerol oxidation with the effect of the amount of catalyst is shown in Figure 7. As can be seen, high percentages in the decrease of glycerol are not obtained at the end of the reaction time, achieving conversions between 6 and 15%, approximately, with the three amounts of Cu/TiO<sub>2</sub> in 6 h. Although oxidation is slow, an increase in the conversion can be observed with the increase in the catalyst loading, which is related to a greater area available for photon absorption during catalytic activation by the effect of radiation, which leads to a high rate of hydroxyl radical generation. Similarly, the catalyst load could increase the number of photogenerated active sites for the adsorption of organic molecules [22,24]. Likewise, a considerable increase in the initial reaction rate was observed when using a higher catalyst loading (0.4 g/L), obtaining a value of  $19.8 \times 10^{-4}$  mol/L h. In photocatalysis, a decay trend in the degradation rate may be related to an excess in the amount of catalyst, which reduces the penetration of radiation due to the opacity of the solution [47]. In this study, such maximum catalyst loading limit is not exceeded. It is also worth noting that the maximum catalyst concentration used in this work is one order of magnitude lower than other studies where 100% conversion has been reported with catalysts such as Au/TiO<sub>2</sub> and using a lamp with higher intensity (100 W) than the used here (8 W) [24].

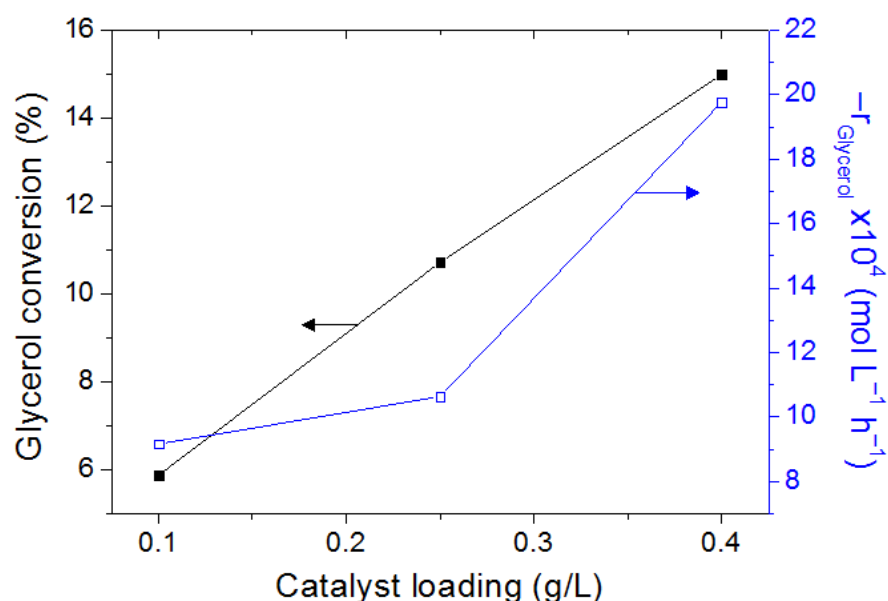


**Figure 7.** Effect of catalyst concentration on glycerol conversion and initial reaction rate (Initial glycerol concentration =  $6.25 \times 10^{-2}$  M, T = 305.65 K, Cu/TiO<sub>2</sub> catalyst).

The concentration and selectivity of glycerol oxidation products when using different catalyst concentrations are shown in Figure 8. As can be seen, the compounds formed during the oxidation of glycerol are glyceraldehyde (GCD), formaldehyde (FD), and formic acid (FA). When the amount of catalyst is low (0.1 g/L), the lowest generation of products is obtained. On the other hand, when the catalyst loading is the highest (0.4 g/L), a maximum concentration can be observed. A high concentration of product formation associated with high amount of catalyst may be related to higher generation of hydroxyl radicals, as shown in Equations (1)–(3), which are the main species responsible for the oxidation of the organic molecule [48]. Likewise, copper species can act as electron traps by reducing the

recombination rate of photogenerated electron/hole pairs, as can be seen in Equation (4), thus increasing the generation of  $\bullet\text{OH}$  radicals [49],

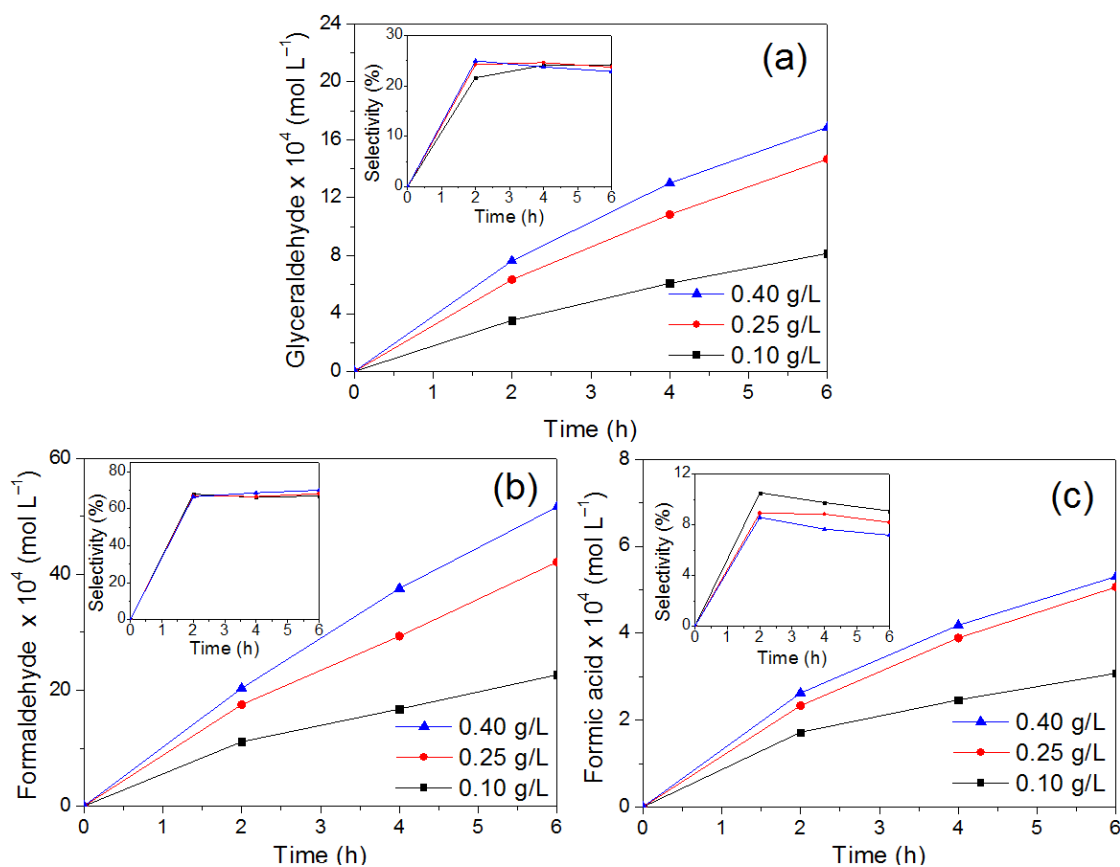
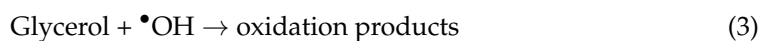


**Figure 8.** Effect of catalyst amount on concentration and selectivity towards (a) glyceraldehyde (GCD), (b) formaldehyde (FD), and (c) formic acid (FA). Initial glycerol =  $6.25 \times 10^{-2}$  M, T = 305.65 K, Cu/TiO<sub>2</sub> catalyst.

Figure 8a shows the GCD concentration profiles with a maximum concentration at 6 h of reaction for all catalyst loadings, as a result of oxidation. The formation of glyceraldehyde is related to the attack of hydroxyl radicals on the glycerol molecule in the C1 position in comparison with the reactivity in the C2 position towards the formation of dihydroxyacetone [50]; however, in this study, the generation of dihydroxyacetone was negligible since the abstraction of the first hydrogen is favored (see Figure 9) [51]. The subsequent oxidation of glyceraldehyde by hydroxyl radicals can form other byproducts, such as formic acid and formaldehyde, this is due to the incision of the C-C bonds in the organic molecule [46]. Figure 8b,c shows the concentration profiles of the formaldehyde and formic acid formed during the photo-oxidation tests, respectively. Both products show an increasing trend over time for each catalyst amount, but with 0.4 g/L of catalyst the greatest generation is observed. FD was the product with the highest concentration of formation compared to GCD and FA, showing a selectivity of up to 65%, as shown in Figure 8.

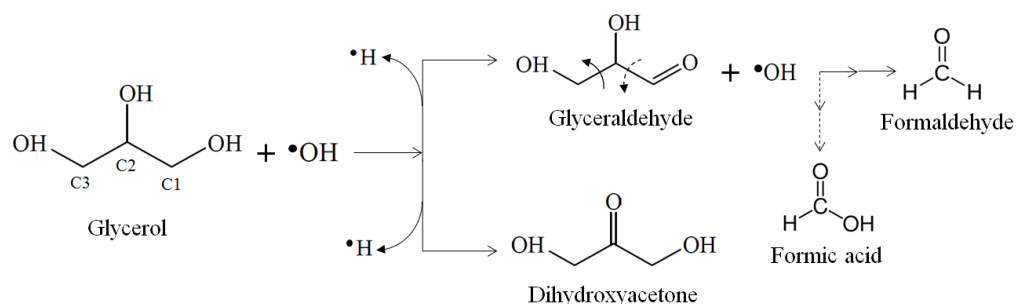


**Figure 9.** Proposed reaction scheme for the photo-oxidation of glycerol by Cu/TiO<sub>2</sub>.

### 2.2.2. Effect of Reaction Temperature

The effect of reaction temperature was studied in the range of 298.15–313.15 K while keeping the concentration of catalyst (0.25 g/L) and glycerol ( $6.25 \times 10^{-2}$  M) constant. Figure 10 shows the glycerol conversion and initial reaction rate with different temperatures on the photo-oxidation reactions. As can be seen, the increase in temperature promotes the degradation of glycerol, achieving a conversion of 21% at 313.15 K in 6 h. This is related to a greater molecular excitation that favors the interaction of the glycerol molecules and the catalyst, which increases the catalytic activity [52]. Likewise, initial reaction rates are favored by the increase in temperature. The decrease in glycerol concentration due to evaporation from solution is considered negligible.

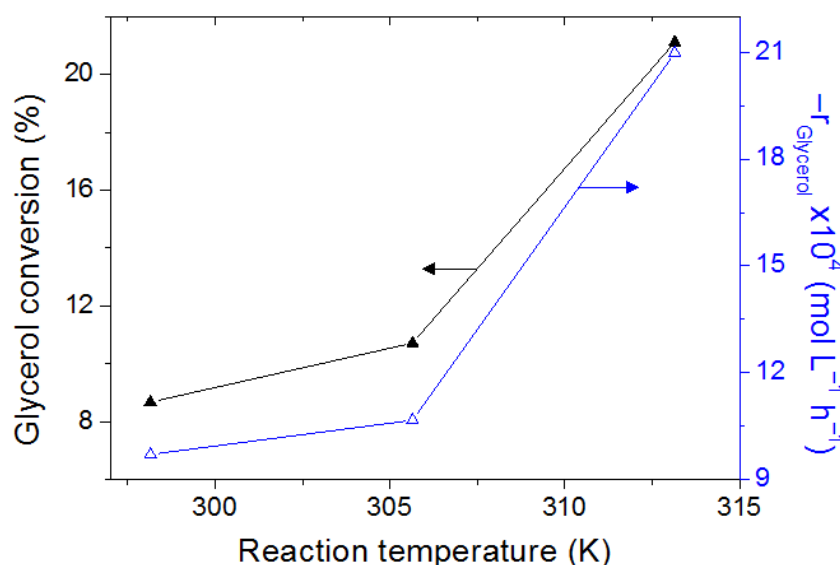


**Figure 10.** Effect of reaction temperature on the glycerol conversion and initial reaction rate (initial glycerol =  $6.25 \times 10^{-2}$  M, Cu/TiO<sub>2</sub> = 0.25 g/L).

Figure 11 shows the effect of reaction temperature on concentration and selectivity of the products formed during glycerol photo-oxidation. It is worth noticing that the accumulation of GCD is favored by the increase of temperature, see Figure 11a, which is associated with an increase in the oxidation rate of glycerol [53]. These results indicate the reaction, beyond temperatures of 305 K, is being photo- and thermo-activated. The GCD concentration increases 57% as the temperature increases from 298.15 K to 313.15 K after 6 h of reaction due to high oxidation. This is supported by the fact that the production rates of the secondary products (FD and FA), see Figure 11b,c, increase according to temperature. The selectivity of these products remained practically constant with the increase in temperature with values around 69% and 8% for FD and FA, respectively. In the case of GCD, the selectivity decreases with high temperature and this can be ascribed to the presumed increase in its oxidation rate. The maximum concentration of 7.06 mM was

obtained for formaldehyde compared to the glyceraldehyde (1.91 mM) and formic acid (0.73 mM) products at 313.15 K.

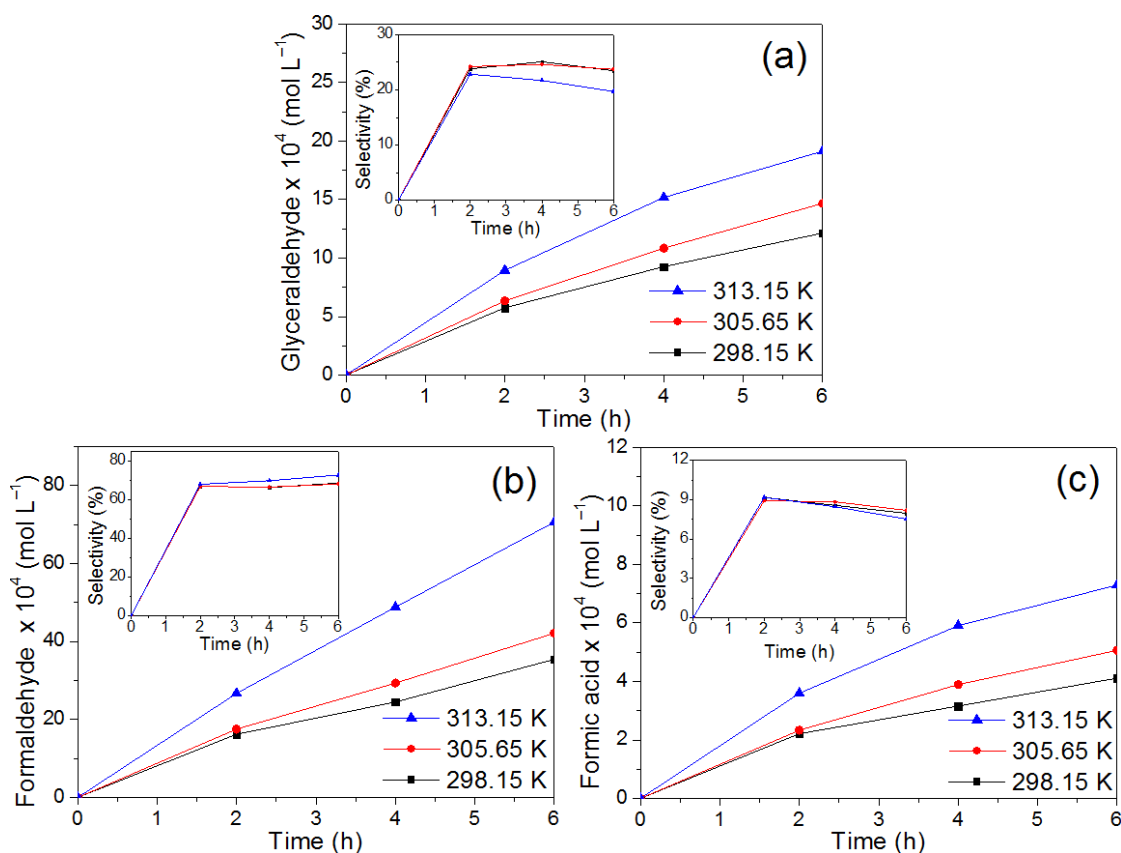


**Figure 11.** Effect of reaction temperature on concentration and selectivity towards (a) glyceraldehyde (GCD), (b) formaldehyde (FD), and (c) formic acid (FA). Initial glycerol =  $6.25 \times 10^{-2}$  M, Cu/TiO<sub>2</sub> = 0.25 g/L.

### 2.2.3. Effect of Initial Glycerol Concentration

The effect of the initial glycerol concentration on the conversion percentage and initial reaction rate of this organic compound is shown in Figure 12. As can be seen, the reaction rate increases from  $1.39 \times 10^{-4}$  mol/L h to  $31.16 \times 10^{-4}$  mol/L h when the initial glycerol concentration is quadrupled from 0.025 M to 0.10 M, which is related to a high oxidation at the beginning of the reaction due to the presence of a greater amount of organic glycerol molecules. A decrease in the amount of glycerol was also observed for the three tested concentrations due to oxidative processes. Low glycerol concentrations (25 mM) exhibited higher percentages of decrease (23.2%) when compared to high initial concentrations (100 mM) that showed a decrease of 9.7%. This behavior is associated with a saturation effect on the active sites of the catalyst, which reduces the activity [54].

The products formed with an effect on the initial glycerol concentration are shown in Figure 13. In this figure, it is observed that the formation of GCD is favored at high concentrations of glycerol and long reaction times. The maximum formation of GCD and selectivity were obtained of 1.53 mM and 30%, respectively, with a glycerol concentration of  $10 \times 10^{-2}$  mol/L at 6 h of reaction, as shown in Figure 13a. On the other hand, the generation of formaldehyde is not directly related to the increase in glycerol concentration, because its maximum concentration was obtained by using the intermediate initial concentration of  $6.25 \times 10^{-2}$  mol/L, as can be seen in Figure 13b. With respect to formic acid, a considerable effect was not observed with the initial amount of glycerol; however, an increase in selectivity occurs when a high initial concentration of glycerol is used according to Figure 13c. Both FD and FA were identified from low glycerol concentrations as they

are secondary reaction products. Formaldehyde is the reaction product that exhibited the highest formation with a concentration of 4.2 mM. Although other products generated during the oxidation of glycerol have been reported by other investigations (glycolic and glyceric acids) as precursor compounds of formaldehyde and formic acid [31,55], in this study, such products were not identified.

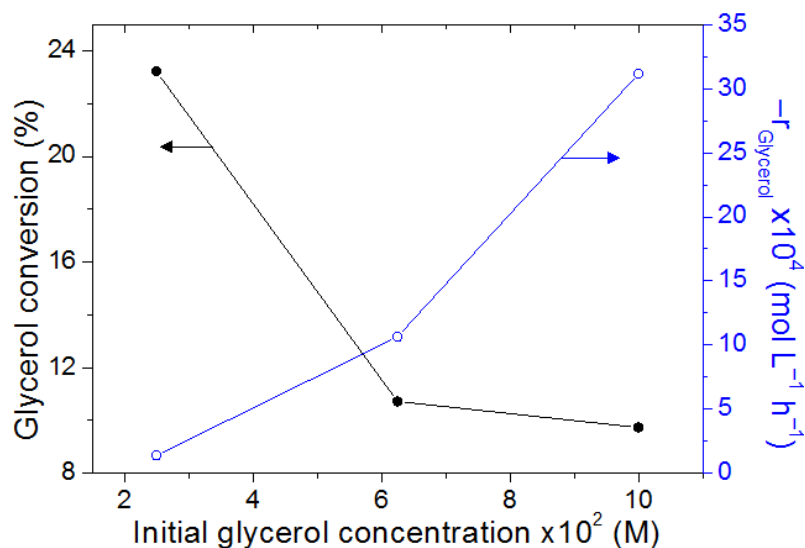


**Figure 12.** Effect of initial glycerol concentration on the glycerol conversion and initial reaction rate ( $T = 305.65$  K,  $\text{Cu}/\text{TiO}_2 = 0.25$  g/L).

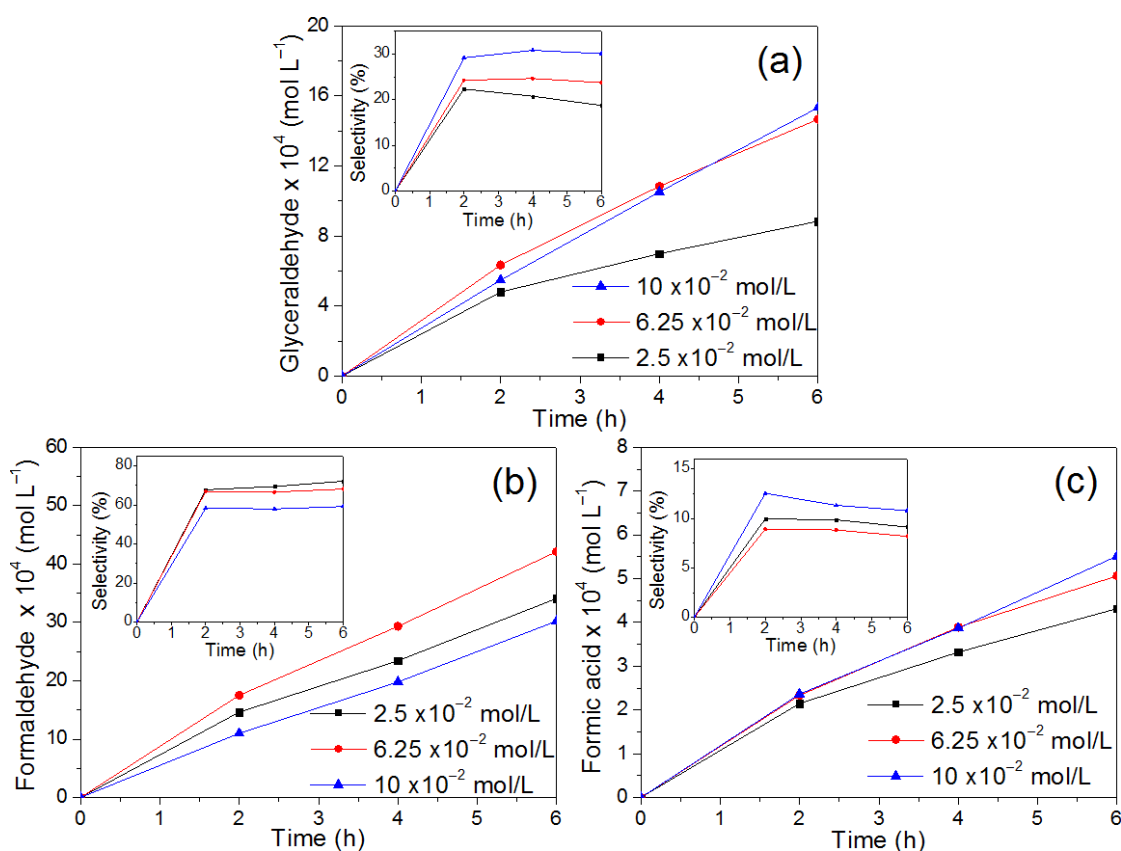


**Figure 13.** Effect of initial glycerol concentration on the selectivity and concentration of (a) glyceraldehyde (GCD), (b) formaldehyde (FD), and (c) formic acid (FA).  $T = 305.65$  K,  $\text{Cu}/\text{TiO}_2 = 0.25$  g/L.

### 2.2.4. Total Organic Carbon Content

In order to evaluate the degree of mineralization during the glycerol photo-oxidation tests, measurements of the total organic carbon (TOC) content were carried out and the results are shown in Figure 14. As can be seen, the deep oxidation of glycerol towards  $\text{CO}_2$  and  $\text{H}_2\text{O}$  was not achieved with respect to the variables studied. However, when a reaction temperature of 313.15 K is used, the maximum change in the TOC value is achieved with a decrease of 10% after 6 h of reaction, as can be seen in Figure 14b. This phenomenon is related to the high oxidation of the organic molecule, as well as of the intermediate compounds.

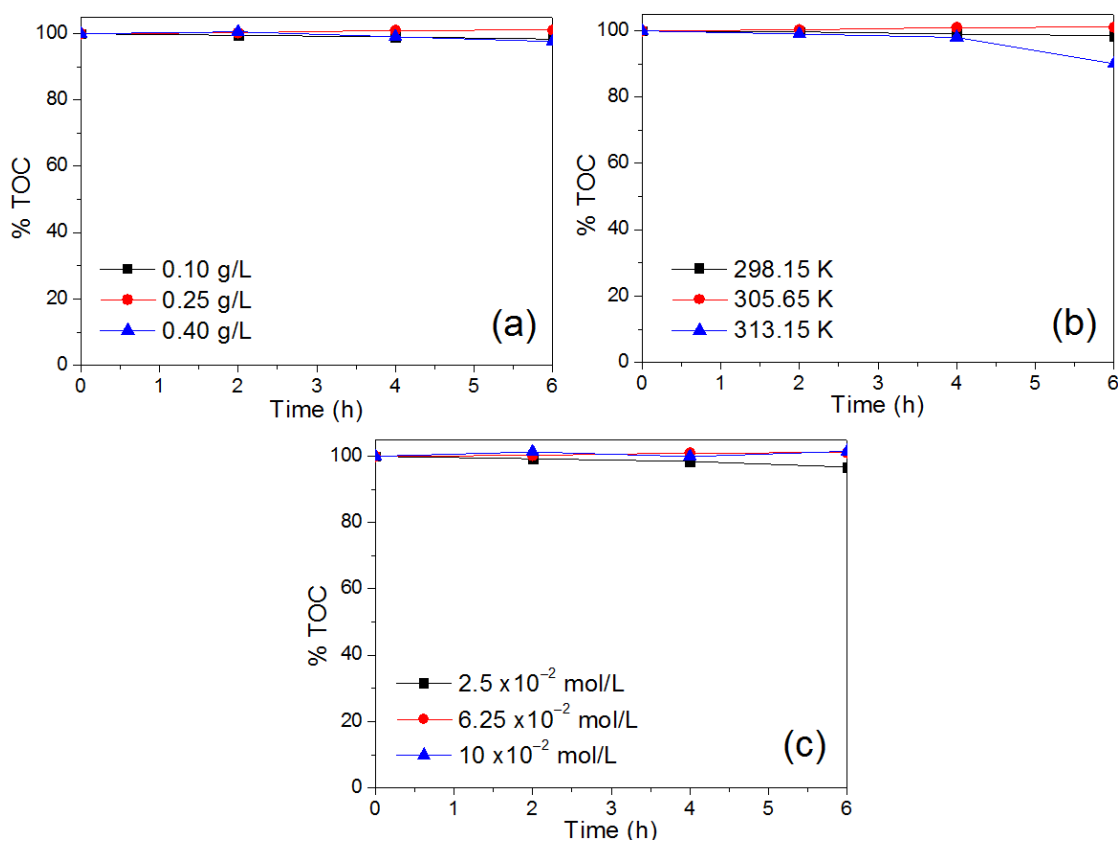


**Figure 14.** Percentage of total organic carbon during glycerol photo-oxidation with effect on (a) amount of catalyst, (b) reaction temperature, and (c) initial glycerol concentration.

### 2.2.5. Optimization

The experimental design for the optimization of the independent variables, catalyst amount ( $X_1$ ), reaction temperature ( $X_2$ ), and glycerol concentration ( $X_3$ ), towards the concentration of the products is shown in Table 4. The polynomial equation for each response variable with its corresponding coefficients calculated from the experimental values using the response surface methodology is shown in Equations (5)–(7).

$$\text{Sqrt}(\text{GCD} \times 10^4) = 301.49 + 11.25X_1 - 1.95X_2 - 423.22X_3 - 11.98X_1^2 + 0.003X_2^2 - 216.90X_3^2 - 0.017X_1X_2 + 51.06X_1X_3 + 1.48X_1X_3 \quad (5)$$

$$\text{Sqrt}(\text{FD} \times 10^4) = 1133.21 - 25.54X_1 - 7.44X_2 - 435.56X_3 - 22.88X_1^2 + 0.012X_2^2 - 582.62X_3^2 + 0.137X_1X_2 + 40.26X_1X_3 + 1.62X_1X_3 \quad (6)$$

$$\text{Sqrt}(\text{FA} \times 10^4) = 318.16 + 6.48X_1 - 2.08X_2 - 239.91X_3 - 6.40X_1^2 + 0.003X_2^2 + 28.46X_3^2 - 0.012X_1X_2 + 26.49X_1X_3 + 0.764X_1X_3 \quad (7)$$

**Table 4.** Experimental design with independent variables and response variables for the selective photo-oxidation of glycerol.

Run	Independent Variables			Response Variables		
	Catalyst Concentration (g/L)	Reaction Temperature (K)	Glycerol Concentration (mol/L)	GCD × 10 <sup>4</sup> (mol/L)	FD × 10 <sup>4</sup> (mol/L)	FA × 10 <sup>4</sup> (mol/L)
1	0.40	313.15	0.0250	10.103	58.834	5.582
2	0.10	313.15	0.1000	17.648	36.328	7.507
3	0.10	305.65	0.0625	8.151	22.669	3.078
4	0.40	298.15	0.1000	13.772	25.308	4.762
5	0.25	298.15	0.0625	12.132	35.432	4.112
6	0.40	305.65	0.0625	16.862	51.647	5.304
7	0.40	298.15	0.0250	8.532	33.806	4.221
8	0.25	305.65	0.0625	14.667	42.121	5.061
9	0.10	298.15	0.0250	6.078	17.491	3.725
10	0.25	305.65	0.0625	14.697	42.160	5.079
11	0.25	305.65	0.0250	8.844	34.104	4.316
12	0.25	305.65	0.0625	14.637	42.082	5.043
13	0.25	305.65	0.0625	14.691	42.178	5.067
14	0.10	298.15	0.1000	4.863	8.761	2.309
15	0.25	313.15	0.0625	19.129	70.601	7.295
16	0.25	305.65	0.0625	14.644	42.065	5.055
17	0.10	313.15	0.0250	8.391	34.685	5.517
18	0.25	305.65	0.0625	14.731	42.273	5.089
19	0.25	305.65	0.1000	15.338	30.237	5.513
20	0.40	313.15	0.1000	32.834	84.294	11.613

The analysis of variance (ANOVA), as can be seen in Table S1 of the Supplementary Information, suggests a quadratic polynomial model with a square root transform for a better representation of the experimental data according to the value obtained from the coefficient of determination ( $R^2$ ), with values of 0.9908, 0.9949, and 0.9857 for the response variables GCD, FD, and FA, respectively.  $R^2$  values close to unity indicate a better fit of the data; otherwise small values indicate that the response values are not adequate to explain the behavior [56]. The values of the determination coefficients obtained in our study are higher than 0.7, therefore the effect of the independent variables on the response values can be appropriately described by the quadratic polynomial model (Fit Statistics can be seen in Table S1).

Pareto analysis was performed according to Equation (8) in order to determine the percentage effect of each factor ( $P_i$ ) on the responses,

$$P_i = \left( \frac{\alpha_i}{\sum_i \alpha_i} \right) \times 100 \quad (8)$$

Figure 15 shows the Pareto graphic analysis. The results in this figure suggest that among the variables,  $\alpha_3$  (glycerol concentration, mol/L) produces the largest effect: 41.52%, 19.36%, and 38.16% on all responses (GCD, FD, and FA), respectively. Moreover, the interaction term  $\alpha_{13}$  (catalyst amount (g/L)\*glycerol concentration (mol/L)), produces a medium effect 5.01%, 1.79%, and 4.21% on all responses (GCD, FD, and FA), respectively.

In order to observe the influence of the amount of catalyst, reaction temperature, and glycerol concentration on the response variables (products concentration), 3D plots are shown in Figure 16 by keeping one independent variable constant (at the central value) and varying the other two variables within the studied range. Figure 16a,d,g shows the change in reaction temperature and amount of catalyst with a constant glycerol concentration of 0.0625 mol/L, Figure 16b,e,h presents the variation in glycerol concentration and catalyst amount with a constant reaction temperature of 305.65 K, and Figure 16c,f,i exhibits the change in glycerol concentration and reaction temperature with a constant catalyst amount of 0.25 g/L, which allows to graphically observe the interaction of all the independent variables involved in this study.

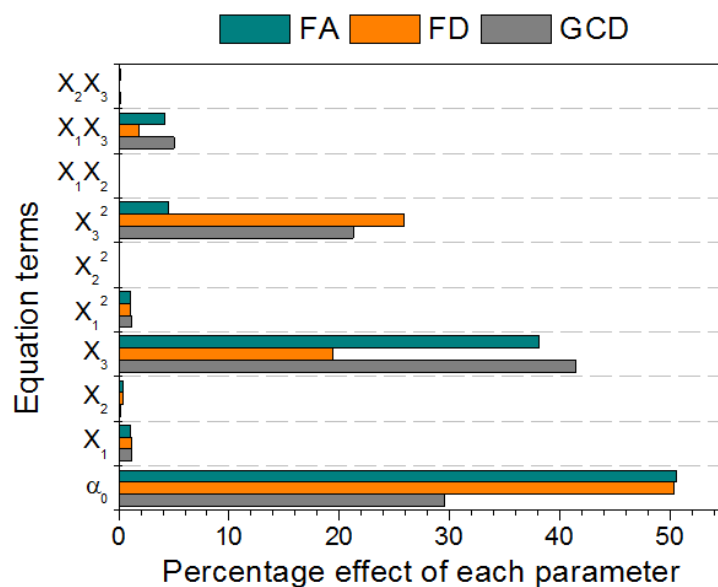


Figure 15. Pareto chart analysis.

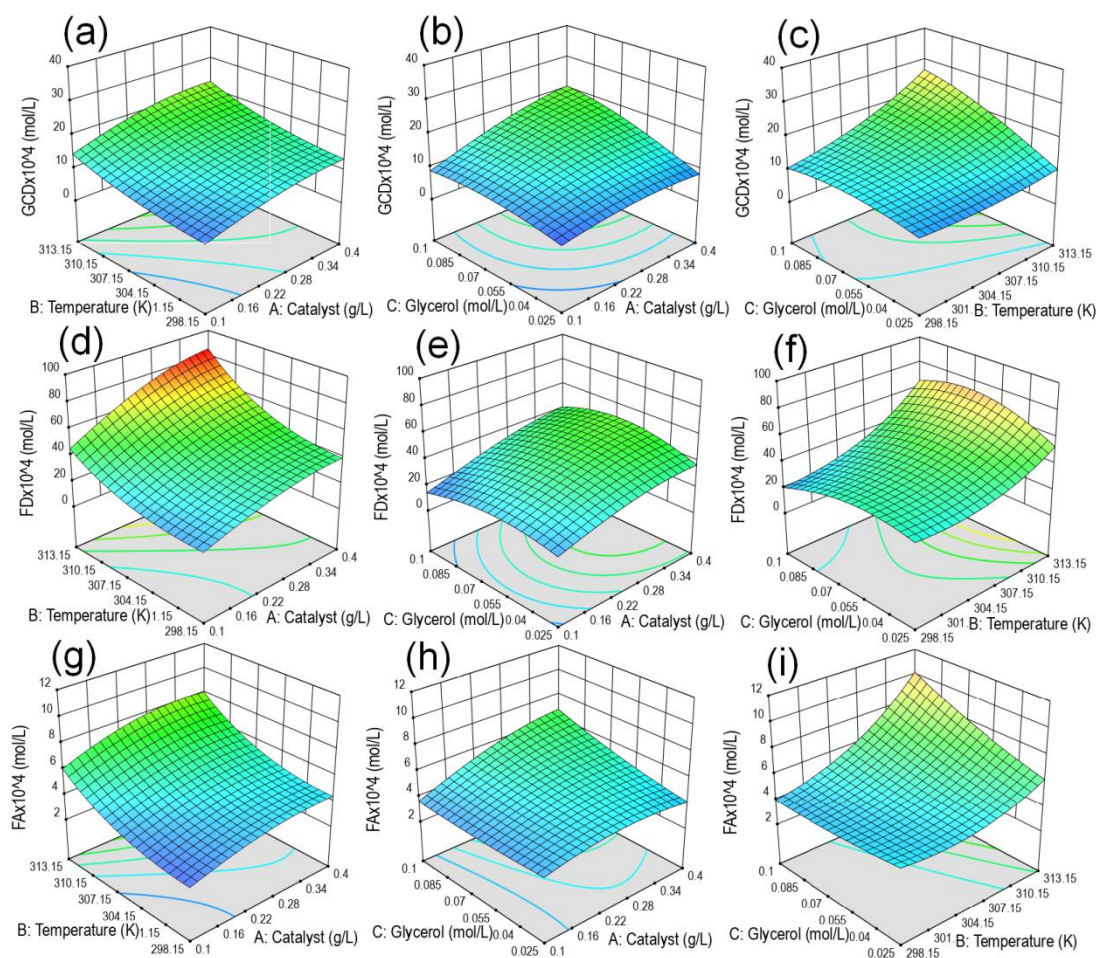


Figure 16. Response surface plots for all possible combinations when two independent variables change and the other variable remains constant at the center point. (a,d,g) show the change in reaction temperature and catalyst amount with a constant glycerol concentration. (b,e,h) show the variation in glycerol concentration and catalyst amount with a constant reaction temperature. (c,f,i) show the change in glycerol concentration and reaction temperature with a constant catalyst amount.

The optimization of the values for the response variables is shown in Table 5. The optimization was carried out considering as objective goal the maximization of the GCD, FD, and FA products within the entire range of values of the independent variables. The result obtained with the highest desirability (0.984) was selected as the optimum point. The optimized reaction conditions were using a catalyst amount of 0.4 g/L, reaction temperature of 313.15 K, and glycerol concentration of 0.1 mol/L. The values of the response variables at the optimal conditions were  $32.27 \times 10^{-4}$ ,  $81.74 \times 10^{-4}$ , and  $11.47 \times 10^{-4}$  mol/L for GCD, FD, and FA, respectively.

**Table 5.** Optimum and experimental values of the response variables.

Response Variables	Optimum $\times 10^4$ (mol/L)	Experimental $\times 10^4$ (mol/L)
Glyceraldehyde (GCD)	32.267	32.834
Formaldehyde (FD)	81.741	84.294
Formic acid (FA)	11.465	11.613

The optimal reaction conditions towards the maximization of the products were evaluated using  $\text{TiO}_2 + \text{UV}$ , UV and visible light ( $\lambda > 400 \text{ nm}$ ), and the results are shown in Figure 17. Therefore, the photocatalytic activity during glycerol oxidation is lower in all processes compared to the  $\text{Cu}/\text{TiO}_2 + \text{UV}$  system. The absence of copper species in titania ( $\text{TiO}_2 + \text{UV}$  system) significantly reduces the concentration of the products, which is due to the fact that copper acts as an electron trap, see Equation (4), by reducing the recombination of photogenerated charges, which increases the formation of the main oxidative species (hydroxyl radicals). It can also be observed in Figure 17 that the glycerol oxidation also proceeds with UV light only. This might be due to the production of hydroxyl radicals from hydrogen peroxide that is being produced via the following two reactions [51],

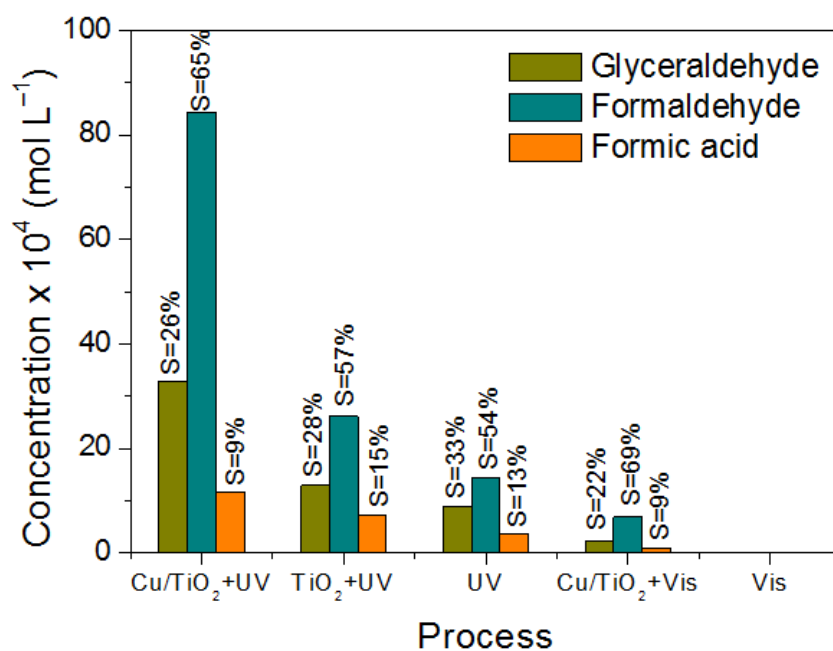


**Figure 17.** Comparison of the best reaction conditions using UV and visible light towards the concentration and selectivity of products during the glycerol selective oxidation.

The generation of  $H_2O_2$  was previously proven in the same reaction system, i.e., lamp and reactor [51]. Once the  $H_2O_2$  is formed, this might be dissociated into hydroxyl radicals (responsible of glycerol oxidation) by a Fenton-like mechanism favored by the presence of Cu [51]. The proton that is activated for reaction (9) to proceed is believed to come from the interaction of an energetic enough light source and glycerol [51]. The oxygen in reaction (9) is the one in solution.

Thus, by contrasting the results in Figure 17, the photocatalytic effect of the synthesized material can be concluded. No effect of photolysis with visible radiation was observed.

On the other hand, only glycerinaldehyde was obtained as a primary oxidation product with a concentration of  $2.22 \times 10^{-4}$  mol/L when using Cu/TiO<sub>2</sub> + visible light, and a low concentration of formaldehyde ( $6.92 \times 10^{-4}$  mol/L) and formic acid ( $0.92 \times 10^{-4}$  mol/L) as secondary products compared to those obtained with Cu/TiO<sub>2</sub> + UV radiation ( $84.29 \times 10^{-4}$  mol/L and  $11.61 \times 10^{-4}$  mol/L, respectively), according to the scheme proposed in Figure 9. This behavior is related to the low activation of the catalyst, since the visible radiation did not provide enough energy to generate a greater number of electron/hole pairs (see Figure S2), despite the fact that the semiconductor presented a reduction in the band-gap energy (see Table 2), which has been reported in other investigations [38–40]. However, the selectivity towards formaldehyde is favored by using visible radiation (69%) instead of UV light (65%), as can be seen in Figure 17. The pH before (5.8) and after (3.6) the process for the Cu/TiO<sub>2</sub> + UV system suggests the generation of acid species, in this case the formation of formic acid as a secondary product during the photo-oxidation of glycerol [57].

The stability of the synthesized Cu/TiO<sub>2</sub> catalyst was evaluated under optimal reaction conditions using two catalyst reuse cycles. The TOC content was evaluated after each cycle and the results are shown in Figure 18. As can be seen, there is no change in the TOC value at the end of each cycle, which is related to the partial oxidation of glycerol without reaching a deep level of oxidation in terms of mineralization in each reuse. This is a relevant result since mineralization is a main cause of selectivity loss reported in other works [58]. Although H<sub>2</sub> has been identified and quantified as a product from the photocatalytic oxidation of glycerol [21,27], in this study, the investigation was centered only on the generated organic products.

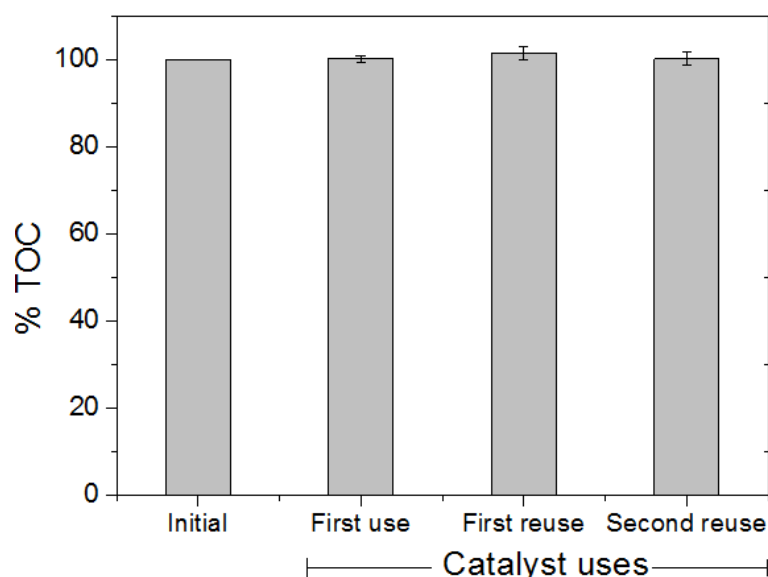
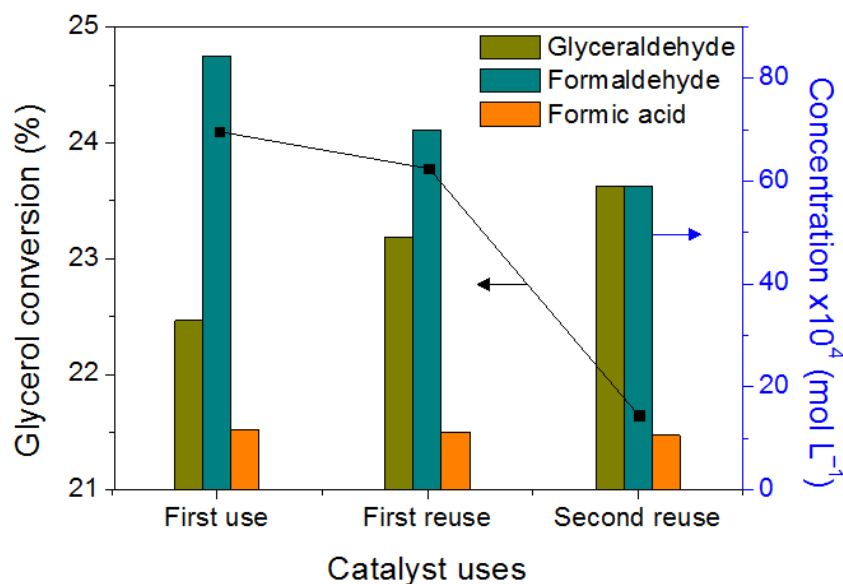


Figure 18. TOC percentage at the end of each catalyst reuse cycle.

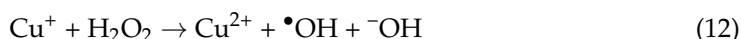
The percentage of glycerol degradation and distribution of products formed for each reuse cycle are shown in Figure 19. During the catalyst recycling experiments, a decrease of only 2.5% in the percentage of glycerol degradation can be observed. This decrease can be ascribed to the inherent experimental error and to catalyst loss during sampling and

recovery in each cycle [59]. The oxidation towards formaldehyde as secondary reaction product is also diminished and the accumulation of glyceraldehyde, as a primary product, is increased after each reuse cycle.



**Figure 19.** Glycerol degradation percentage and product concentration for different Cu/TiO<sub>2</sub> catalyst reuse cycles.

The main species involved in the oxidation of organic molecules were evaluated. The effect of scavengers of holes and hydroxyl radicals was studied on the percentage of glycerol degradation and the results are shown in Figure 20. As can be seen in Figure 20, the presence of methanol (MeOH) in the reaction system as a hole scavenger [60,61] inhibits the conversion of glycerol to approximately 7%. Similarly, the introduction of salicylic acid (SA) as a scavenger of hydroxyl radicals [62] inhibits the conversion of glycerol to a greater extent. The almost null conversion using SA confirms that hydroxyl radicals are the dominant oxidative species, whose generation is through reactions (2), (12), (13) and (14). In addition, the results when using MeOH suggest that holes on the titania surface are also reactive species in the glycerol oxidation. On the other hand, the electron trapped by the copper species can be scavenged by the oxygen present and by the hydrogen peroxide formed [38], thus generating other reactive species by reactions (11) and (12), which becomes a cycle of electron capture and donation during photocatalytic activation. The presence of Cu<sup>2+</sup> species after the catalyst first use was corroborated by XPS analysis (see Figure S3).



The production rate values for GCD and FD obtained with TiO<sub>2</sub> and other metal/TiO<sub>2</sub> catalysts are summarized in Table 6. Formic acid was not considered in this table because it was not quantified in the related literature. It is worth pointing out that the comparison should be taken with caution since the values reported in Table 6 were obtained under a different radiation field and a reactor completely different to that used in this work. At this point, it is worth recalling that the radiation intensity and reactor design affect oxidation rate [63]. Nevertheless, it is important to notice that the accumulation rate of GCD and FD in this work is one and two orders of magnitude higher, respectively, than

in previous studies where the glycerol photo-oxidation is catalyzed by other metals. It is worth clarifying that it was decided to use the term accumulation rather than production because it is likely that those values are reflecting the rate of production and consumption. This is because oxidation is acknowledged to proceed via the attack of hydroxyl radicals, which are not selective at all. Thus, these radicals may be attacking the glycerol molecule and concomitantly, albeit at a different rate, the oxidation products such as GCD and FD in such a way that a higher amount of available hydroxyl radicals will be reflected in a higher oxidation degree of all molecules, which will also decrease the concentration of all of them. Therefore, the values in Table 6 suggest that Cu/TiO<sub>2</sub> is not more active than the other catalysts but is more selective by “dosing” the hydroxyl radical production.

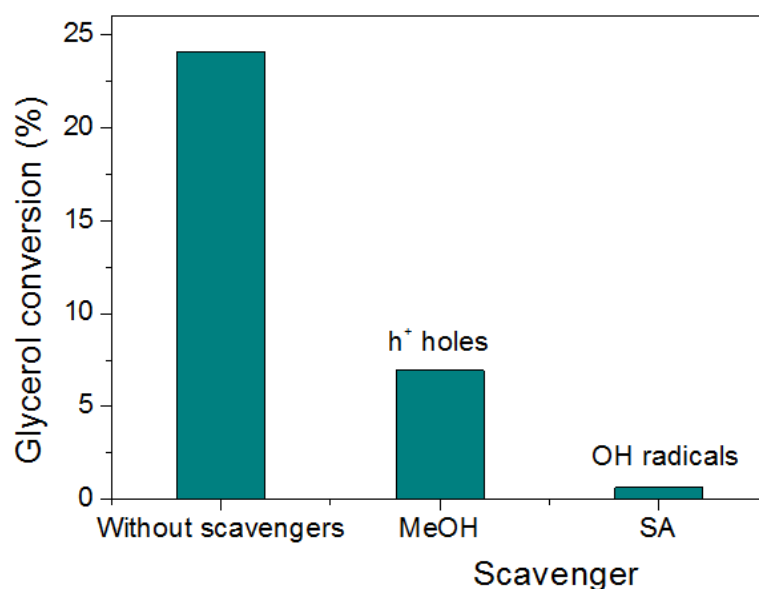


**Figure 20.** Percentage of glycerol converted in the presence of radical and hole scavengers.

**Table 6.** Comparison of accumulation rate of glycerinaldehyde (GCD) and formaldehyde (FD) with TiO<sub>2</sub>, Cu/TiO<sub>2</sub> and other metal-decorated TiO<sub>2</sub>.

Catalyst	Product	mol × 10 <sup>4</sup> /g <sub>cat</sub> ·h	Reference
Pt/TiO <sub>2</sub>	GCD	11.000	[21]
Ag-AgBr/TiO <sub>2</sub>	GCD	3.250	[22]
TiO <sub>2</sub>	GCD	0.934	
	FD	0.233	
Bi/TiO <sub>2</sub>	GCD	0.807	
	FD	0.339	
Pd/TiO <sub>2</sub>	GCD	1.255	[24]
	FD	0.388	
Pt/TiO <sub>2</sub>	GCD	1.680	
	FD	0.425	
Au/TiO <sub>2</sub>	GCD	1.279	
	FD	0.504	
Cu/TiO <sub>2</sub>	GCD	13.681	This work
	FD	35.122	

Based on the results found with the Cu/TiO<sub>2</sub> catalyst presented in this work, it can be said that one of its advantages over the other TiO<sub>2</sub>-based catalysts presented in Table 6, is

to attain a high selectivity towards formaldehyde and glyceraldehyde without using an expensive metal as platinum. Another advantage is its capability of being re-used.

### 3. Materials and Methods

#### 3.1. Synthesis of Photocatalysts

The synthesis through the EISA approach was carried out according to the following methodology: titanium butoxide ( $\text{Ti}(\text{OC}_4\text{H}_9)_4$ ) was added to ethanol ( $\text{C}_2\text{H}_6\text{O}$ ) to form a sol, then a surfactant (copolymer P123) was incorporated and the mixture was kept under stirring for 30 min. Subsequently, the copper precursor ( $\text{Cu}(\text{NO}_3)_2 \cdot 3\text{H}_2\text{O}$ ) was added in a ratio of 5 at.% Cu with respect to the Ti species, and finally nitric acid ( $\text{HNO}_3$ ) was dropwise added. The mixture was kept under constant stirring for 3 h, dried in a rotary evaporator, and calcined at 400 °C for 4 h with an intermediate stage at 300 °C for 1 h and a rate of 1 °C/min. Titanium precursor, solvent, surfactant, and acid were used in a molar ratio of  $5.8 \times 10^{-3}$ : $1.085 \times 10^{-1}$ : $1.03 \times 10^{-4}$ : $2.06 \times 10^{-2}$ , respectively. Cu-free  $\text{TiO}_2$  was synthesized by the same methodology for comparative purposes.

#### 3.2. Characterization

X-ray diffraction (XRD) was used to characterize the synthesized materials using a Bruker diffractometer (Advanced D8, Billerica, MA, USA) with  $\text{K}\alpha$  radiation and the spectra were recorded in  $2\theta$  degrees between 22–66°. The crystal size ( $D$ ) of the nanostructures was estimated by the Debye–Scherrer equation ( $D = k\lambda / \beta \cos \theta$ ), while the distortion of the crystal lattice by  $\epsilon = \beta / 4 \tan \theta$ , where  $k = 0.9$ ,  $\lambda = 1.54 \text{ \AA}$  is the wavelength of the X-ray radiation,  $\theta$  is the diffraction angle, and  $\beta$  is the full-width at half-maximum (FWHM) of the anatase peak.

The textural properties of the catalysts were determined by nitrogen physisorption using Autosorb equipment (Quantachrome, Boynton Beach, FL, USA) at 77 K. The specific surface area and the average pore diameter were estimated by the BET and BJH methods, respectively. Before the analysis, the samples were degassed under vacuum for 2 h at 250 °C.

Band-gap energies were determined by UV–Vis diffuse reflectance spectroscopy (DRS) using a spectrophotometer (Lambda 35, Perkin-Elmer, Waltham, MA, USA) equipped with an integrating sphere (Labsphere RSA-PE-20, North Sutton, NH, USA).

The copper content was determined by atomic absorption spectroscopy (AAS). The solid was dissolved by hydrofluoric acid, diluted in deionized water and analyzed in a Perkin Elmer Spectrophotometer (AAnalyst 200, Waltham, MA, USA).

Images of the crystalline particles were obtained by transmission electron microscopy (TEM) using a JEOL 2100 microscope at 200 kV and with a LaB6 filament (Peabody, MA, USA). The size and shape of the catalytic particles were determined by scanning electron microscopy (SEM) with a JEOL microscope (JSM-6510LV model, Peabody, MA, USA) at 25 kV. Energy dispersive X-ray spectroscopy (EDS) was carried out to estimate the copper composition in the synthesized catalyst using a voltage of 20 kV and a magnification of 550 $\times$ .

Analysis by XPS (X-ray photoelectron spectroscopy) were carried out in a JPS-9200 spectrometer (Peabody, MA, USA) using an Al  $\text{K}\alpha$  radiation source and taking as reference the binding energy of C 1s (284.6 eV).

#### 3.3. Photo-Oxidation of Glycerol

The photo-oxidation reactions of glycerol were conducted in a batch type annular reactor with an internal diameter of 2.5 cm and a height of 20 cm. The radiation source was supplied by a mercury UV lamp of 8 W (Analytik Jena, Upland, CA, USA) placed at the center of the reactor with a typical intensity of 166  $\text{W}/\text{m}^2$  and a primary wavelength of 254 nm. The desired temperature was kept constant inside the reactor during all the photocatalytic tests by means of a thermal bath. A typical reaction was carried out as follows: 0.1 L of glycerol solution was placed in the reactor and then the catalyst was added and kept under constant stirring, finally the UV lamp was turned on to start the catalytic

photo-oxidation, which was maintained for 6 h. Amount of catalyst (0.1, 0.25, and 0.4 g/L), glycerol concentration (0.025, 0.0625, and 0.1 M), and reaction temperature (298.15, 305.65, and 313.15 K) were the studied variables. The best reaction conditions were compared to TiO<sub>2</sub> + UV, UV, and visible light processes. Visible light ( $\lambda > 400$  nm) was supplied by three linear fluorescent lamps (TL5 Essential 14 W/840, Philips Lighting, Amsterdam, the Netherlands). Deionized water was used in all experiments.

### 3.4. Analytical Methods

To assess the glycerol oxidation, several aliquots were removed from the reaction system every 2 h, filtered (nylon membrane 0.2  $\mu$ m) to remove solid particles, and analyzed by ultra high-performance liquid chromatography (UHPLC). The chromatograph (Vanquish) equipped with a RefractoMax 521 Refractive Index Detector (Thermo Scientific, Waltham, MA, USA) was used to identify the glycerol and products obtained after oxidation. The column (5  $\mu$ m, 7.8  $\times$  300 mm, Carbomix Ca-NP, Newark, DE, USA) was kept at 80 °C with a flow rate of 0.6 mL/min (deionized water). For acid compounds, a column (9  $\mu$ m, 7.8  $\times$  300 mm, Aminex HPX-87H, Hercules, CA, USA) at 60 °C and a flow rate of 0.5 mL/min (3 mM H<sub>2</sub>SO<sub>4</sub> solution) was used. The reaction products were quantified using calibration curves.

The Total Organic Carbon (TOC) content was determined with a TOC-L analyzer (Shimadzu, TOC-L CPH/CPN PC-Controlled model, Kyoto, Japan) by catalytic combustion oxidation and infrared identification. Before analysis, 100  $\mu$ L of the previously filtered sample was added to a 10 mL volumetric flask with deionized water. The TOC concentration was determined according to the corresponding calibration curve.

### 3.5. Experimental Design

The effect of the independent variables namely, catalyst amount ( $X_1$ ), reaction temperature ( $X_2$ ), and glycerol concentration ( $X_3$ ) on the concentration of the GCD ( $Y_1$ ), FD ( $Y_2$ ), and FA ( $Y_3$ ) products was studied using the response surface methodology, which follows a face-centered central composite design (FCCCD) with three factors with three levels (see Table 7). Twenty treatments were used randomly according to the central composite design with eight factorial, six axial, and six central points. In addition, a polynomial model of second order was used to evaluate the response values (GCD, FD, and FA concentration) as a function of the independent variables, as shown in Equation (15).

$$Y_i = \alpha_0 + \alpha_1 X_1 + \alpha_2 X_2 + \alpha_3 X_3 + \alpha_{11} X_1^2 + \alpha_{22} X_2^2 + \alpha_{33} X_3^2 + \alpha_{12} X_1 X_2 + \alpha_{13} X_1 X_3 + \alpha_{23} X_2 X_3 \quad (15)$$

where  $Y_i$  represents the values of each response variable, the alpha terms are the coefficients (linear, quadratic, and interactive), and the term  $\alpha_0$  is a constant. The calculation of the coefficients and the statistical parameters were determined using the Design Expert software (version 10.0.8).

**Table 7.** Levels of the independent variables for the selective photo-oxidation of glycerol.

Independent Variables	Levels		
	−1	0	+1
Catalyst amount (g/L)	0.100	0.2500	0.40
Reaction temperature (K)	298.150	305.6500	313.15
Glycerol concentration (mol/L)	0.025	0.0625	0.10

## 4. Conclusions

In this study, titania doped with Cu<sup>2+</sup> cations was successfully prepared using the EISA method. The incorporation of copper doping species doubled the surface area of TiO<sub>2</sub> up to 242 m<sup>2</sup>/g and a reduction of the band gap energy was obtained to a value of 2.55 eV. This method allowed obtaining anatase crystalline phase nanocrystals with average sizes of approximately 8 nm and irregular particle sizes ranging from 30 to 100  $\mu$ m.

The synthesized material proved to be a promising catalyst in selective oxidation during the photocatalytic reaction of glycerol. The compounds formed as a result of the glycerol oxidation were glyceraldehyde, formaldehyde, and formic acid, which are value-added products with industrial importance. The selectivity was favored towards formaldehyde as a secondary product, compared to glyceraldehyde, which is the primary product during glycerol oxidation. Complete oxidation of the glycerol molecule was not observed.

The response surface methodology was used to optimize the independent variables (catalyst amount, reaction temperature, and glycerol concentration) and their relationship with the response variables (product concentration). The optimal conditions towards the maximization of the products considering the desirability function were achieved with the highest values of the independent variables (catalyst loading = 0.4 g/L, glycerol concentration = 0.1 mol/L, and temperature 313.15 K), obtaining concentrations for glyceraldehyde, formaldehyde, and formic acid of 3.23, 8.17, and 1.15 mM, respectively. Under these conditions, the Cu/TiO<sub>2</sub> + UV system was superior to the TiO<sub>2</sub> + UV, UV, and Cu/TiO<sub>2</sub> + Vis processes. The selectivity towards formaldehyde was improved with visible radiation under the optimal reaction conditions. It was found that glycerol oxidation photo-catalyzed by Cu/TiO<sub>2</sub> proceeds mainly by hydroxyl radicals attack.

The independent variable affecting the most of responses is glycerol concentration and therefore special attention should be given to such a variable. The synthesized catalyst exhibits an excellent capability for being re-used.

**Supplementary Materials:** The following supporting information can be downloaded at: <https://www.mdpi.com/article/10.3390/catal12080835/s1>, Figure S1: Energy Dispersive Spectroscopy analyzes for the Cu/TiO<sub>2</sub> catalyst; Figure S2: Photometric spectrum of the visible radiation lamp used during the photocatalytic tests; Figure S3: XPS spectra of (a) Ti 2p, (b) O 1s, and (c) Cu 2p for the Cu/TiO<sub>2</sub> catalyst after first use; Table S1: ANOVA for Quadratic model.

**Author Contributions:** Conceptualization, R.N. and O.A.-G.; methodology, R.N., S.L.M.-V., J.E.-V. and A.M.-Z.; software, S.L.M.-V. and A.R.-M.; validation, O.A.-G.; formal analysis, R.N., S.L.M.-V. and O.A.-G.; investigation, O.A.-G. and A.M.-Z.; resources, R.N., R.R. and J.E.-V.; data curation, A.R.-M. and O.A.-G.; writing—original draft preparation, O.A.-G.; writing—review and editing, R.N., R.R. and A.R.-M.; visualization, O.A.-G. and A.M.-Z.; supervision, R.N., R.R. and A.M.-Z.; project administration, R.N. and R.R.; funding acquisition, R.N., R.R. and J.E.-V. All authors have read and agreed to the published version of the manuscript.

**Funding:** O. Avilés is grateful to COMECYT–Mexico (CAT2021-0032) and authors are grateful to UAEMex for financial support through project 6518/2022CIB.

**Data Availability Statement:** The data presented in this study are available on request from corresponding author (R.N.).

**Acknowledgments:** Authors are grateful to CCIQS (UAEM-UNAM) for the provided support. The technical support of María Citlalit Martínez Soto is also acknowledged.

**Conflicts of Interest:** The authors declare no conflict of interest.

## References

1. Garlapati, V.K.; Shankar, U.; Budhiraja, A. Bioconversion technologies of crude glycerol to value added industrial products. *Biotechnol. Rep.* **2016**, *9*, 9–14. [[CrossRef](#)] [[PubMed](#)]
2. Bagnato, G.; Iulianelli, A.; Sanna, A.; Basile, A. Glycerol Production and Transformation: A Critical Review with Particular Emphasis on Glycerol Reforming Reaction for Producing Hydrogen in Conventional and Membrane Reactors. *Membranes* **2017**, *7*, 17. [[CrossRef](#)] [[PubMed](#)]
3. Zhang, P.; Yue, C.; Fan, M.; Haryonob, A.; Leng, Y.; Jiang, P. The selective oxidation of glycerol over metal-free photocatalysts: Insights into the solvent effect on catalytic efficiency and product distribution. *Catal. Sci. Technol.* **2021**, *11*, 3385–3392. [[CrossRef](#)]
4. Villa, A.; Jouve, A.; Sanchez Trujillo, F.J.; Motta, D.; Prati, L.; Dimitratos, N. Exploring the Effect of Au/Pt Ratio on Glycerol Oxidation in Presence and Absence of a Base. *Catalysts* **2018**, *8*, 54. [[CrossRef](#)]
5. Li, X.; Zhang, Y. Oxidative Dehydration of Glycerol to Acrylic Acid over Vanadium-Substituted Cesium Salts of Keggin-Type Heteropolyacids. *ACS Catal.* **2016**, *6*, 2785–2791. [[CrossRef](#)]

6. Jedsukontorn, T.; Meeyoo, V.; Saito, N.; Hunsom, M. Route of glycerol conversion and product generation via TiO<sub>2</sub>-induced photocatalytic oxidation in the presence of H<sub>2</sub>O<sub>2</sub>. *Chem. Eng. J.* **2015**, *281*, 252–264. [[CrossRef](#)]
7. Lu, Z.; Demianets, I.; Hamze, R.; Terrile, N.J.; Williams, T.J. A Prolific Catalyst for Selective Conversion of Neat Glycerol to Lactic Acid. *ACS Catal.* **2016**, *6*, 2014–2017. [[CrossRef](#)]
8. Chi, Z.; Pyle, D.; Wen, Z.; Frear, C.; Chen, S. A laboratory study of producing docosahexaenoic acid from biodiesel-waste glycerol by microalgal fermentation. *Process Biochem.* **2007**, *42*, 1537–1545. [[CrossRef](#)]
9. Liu, C.; Hirohara, M.; Maekawa, T.; Chang, R.; Hayashi, T.; Chiang, C.-Y. Selective electro-oxidation of glycerol to dihydroxyacetone by a non-precious electrocatalyst–CuO. *Appl. Catal. B Environ.* **2020**, *265*, 118543. [[CrossRef](#)]
10. Hermes, N.A.; Corsetti, A.R.; Pacheco, A.S.; Lansarin, M.A. Photocatalytic Oxidation of Glycerol over ZnO: Systematic Evaluation of Reaction Parameters. *J. Adv. Oxid. Technol.* **2015**, *18*, 315–321. [[CrossRef](#)]
11. Zhang, Y.; Zhang, N.; Tang, Z.-R.; Xu, Y.-J. Identification of Bi<sub>2</sub>WO<sub>6</sub> as a highly selective visible-light photocatalyst toward oxidation of glycerol to dihydroxyacetone in water. *Chem. Sci.* **2013**, *4*, 1820–1824. [[CrossRef](#)]
12. Ning, X.; Li, Y.; Yu, H.; Peng, F.; Wang, H.; Yang, Y. Promoting role of bismuth and antimony on Pt catalysts for the selective oxidation of glycerol to dihydroxyacetone. *J. Catal.* **2016**, *335*, 95–104. [[CrossRef](#)]
13. Chong, R.; Li, J.; Zhou, X.; Ma, Y.; Yang, J.; Huang, L.; Han, H.; Zhang, F.; Li, C. Selective photocatalytic conversion of glycerol to hydroxyacetaldehyde in aqueous solution on facet tuned TiO<sub>2</sub>-based catalysts. *Chem. Commun.* **2014**, *50*, 165–167. [[CrossRef](#)] [[PubMed](#)]
14. Chen, X.; Xie, Z.; Liang, Y.; Wei, J.; Zhu, Y.; Huo, Y.; Zhang, X.; Wang, H. Hybridizing TiO<sub>2</sub> with Nitrogen-Doped Carbon: A New Route to A Highly Visible Light-Active Photocatalyst. *ChemistrySelect* **2017**, *2*, 1565–1572. [[CrossRef](#)]
15. Cai, Q.; Hu, J. Effect of UVA/LED/TiO<sub>2</sub> photocatalysis treated sulfamethoxazole and trimethoprim containing wastewater on antibiotic resistance development in sequencing batch reactors. *Water Res.* **2018**, *140*, 251–260. [[CrossRef](#)]
16. Jedsukontorn, T.; Saito, N.; Hunsom, M. Photoinduced Glycerol Oxidation over Plasmonic Au and AuM (M = Pt, Pd and Bi) Nanoparticle-Decorated TiO<sub>2</sub> Photocatalysts. *Nanomaterials* **2018**, *8*, 269. [[CrossRef](#)]
17. Islam, S.Z.; Nagpure, S.; Kim, D.Y.; Rankin, S.E. Synthesis and Catalytic Applications of Non-Metal Doped Mesoporous Titania. *Inorganics* **2017**, *5*, 15. [[CrossRef](#)]
18. Husin, H.; Mahidin, M.; Pontas, K.; Ahmadi, A.; Ridho, M.; Erdiwansyah, E.; Nasution, F.; Hasfita, F.; Hussin, M.H. Microwave-assisted catalysis of water-glycerol solutions for hydrogen production over NiO/zeolite catalyst. *Heliyon* **2021**, *7*, e07557. [[CrossRef](#)] [[PubMed](#)]
19. Martín-Gómez, J.; Hidalgo-Carrillo, J.; Montes, V.; Estévez-Toledano, R.C.; Escamilla, J.C.; Marinas, A.; Urbano, F.J. EPR and CV studies cast further light on the origin of the enhanced hydrogen production through glycerol photoreforming on CuO:TiO<sub>2</sub> physical mixtures. *J. Environ. Chem. Eng.* **2021**, *9*, 105336. [[CrossRef](#)]
20. Macedo, M.S.; Soria, M.A.; Madeira, L.M. Process intensification for hydrogen production through glycerol steam reforming. *Renew. Sustain. Energy Rev.* **2021**, *146*, 111151. [[CrossRef](#)]
21. Maslova, V.; Quadrelli, E.A.; Gaval, P.; Fasolini, A.; Albonetti, S.; Basile, F. Highly-dispersed ultrafine Pt nanoparticles on microemulsion-mediated TiO<sub>2</sub> for production of hydrogen and valuable chemicals via oxidative photo-dehydrogenation of glycerol. *J. Environ. Chem. Eng.* **2021**, *9*, 105070. [[CrossRef](#)]
22. Rangarajan, G.; Pal, R.; Farnood, R. Visible light driven selective photocatalytic synthesis of high-value carbonyl compounds from glycerol over Ag-AgBr/TiO<sub>2</sub> nanocomposites in acetonitrile. *Mater. Lett.* **2021**, *292*, 129535. [[CrossRef](#)]
23. Jedsukontorn, T.; Ueno, T.; Saito, N.; Hunsom, M. Narrowing band gap energy of defective black TiO<sub>2</sub> fabricated by solution plasma process and its photocatalytic activity on glycerol transformation. *J. Alloys Compd.* **2018**, *757*, 188–199. [[CrossRef](#)]
24. Jedsukontorn, T.; Saito, N.; Hunsom, M. Photocatalytic behavior of metal-decorated TiO<sub>2</sub> and their catalytic activity for transformation of glycerol to value added compounds. *Mol. Catal.* **2017**, *432*, 160–171. [[CrossRef](#)]
25. Dodekatos, G.; Tüysüz, H. Plasmonic Au/TiO<sub>2</sub> nanostructures for glycerol oxidation. *Catal. Sci. Technol.* **2016**, *6*, 7307–7315. [[CrossRef](#)]
26. Bagheri, S.; Julkapli, N.M.; Yehye, W.A. Catalytic conversion of biodiesel derived raw glycerol to value added products. *Renew. Sustain. Energy Rev.* **2015**, *41*, 113–127. [[CrossRef](#)]
27. Maslova, V.; Fasolini, A.; Offidani, M.; Albonetti, S.; Basile, F. Solar-driven valorization of glycerol towards production of chemicals and hydrogen. *Catal. Today* **2021**, *380*, 147–155. [[CrossRef](#)]
28. Valter, M.; dos Santos, E.C.; Pettersson, L.G.M.; Hellman, A. Partial Electrooxidation of Glycerol on Close-Packed Transition Metal Surfaces: Insights from First-Principles Calculations. *J. Phys. Chem. C* **2020**, *124*, 17907–17915. [[CrossRef](#)]
29. Len, C.; Luque, R. Continuous flow transformations of glycerol to valuable products: An overview. *Sustain. Chem. Processes* **2014**, *2*, 1. [[CrossRef](#)]
30. Grabowska, E.; Marchelek, M.; Paszkiewicz-Gawron, M.; Zaleska-Medynska, A. 3-Metal oxide photocatalysts. In *Metal Oxide-Based Photocatalysis*; Zaleska-Medynska, A., Ed.; Elsevier: Amsterdam, The Netherlands, 2018; pp. 51–209. [[CrossRef](#)]
31. He, Z.; Ning, X.; Yang, G.; Wang, H.; Cao, Y.; Peng, F.; Yu, H. Selective oxidation of glycerol over supported noble metal catalysts. *Catal. Today* **2021**, *365*, 162–171. [[CrossRef](#)]
32. Yang, L.; Li, X.; Chen, P.; Hou, Z. Selective oxidation of glycerol in a base-free aqueous solution: A short review. *Chin. J. Catal.* **2019**, *40*, 1020–1034. [[CrossRef](#)]

33. Mehmood, T.; Ahmed, A.; Ahmad, A.; Ahmad, M.S.; Sandhu, M.A. Optimization of mixed surfactants-based  $\beta$ -carotene nanoemulsions using response surface methodology: An ultrasonic homogenization approach. *Food Chem.* **2018**, *253*, 179–184. [[CrossRef](#)] [[PubMed](#)]
34. Mancuso, A.; Sacco, O.; Vaiano, V.; Sannino, D.; Pragliola, S.; Venditto, V.; Morante, N. Visible light active Fe-Pr co-doped TiO<sub>2</sub> for water pollutants degradation. *Catal. Today* **2021**, *380*, 93–104. [[CrossRef](#)]
35. Avilés-García, O.; Espino-Valencia, J.; Romero, R.; Rico-Cerda, J.L.; Natividad, R. Oxidation of 4-Chlorophenol by Mesoporous Titania: Effect of Surface Morphological Characteristics. *Int. J. Photoenergy* **2014**, *2014*, 210751. [[CrossRef](#)]
36. Prashad Ojha, D.; Babu Poudel, M.; Joo Kim, H. Investigation of electrochemical performance of a high surface area mesoporous Mn doped TiO<sub>2</sub> nanoparticle for a supercapacitor. *Mater. Lett.* **2020**, *264*, 127363. [[CrossRef](#)]
37. Caudillo-Flores, U.; Avilés-García, O.; Alonso-Núñez, G.; Kubacka, A.; Fernández-García, M. Assessing quantitatively charge carrier fate in 4-chlorophenol photocatalytic degradation using globular titania catalysts: Implications in quantum efficiency calculation. *J. Environ. Chem. Eng.* **2021**, *9*, 106074. [[CrossRef](#)]
38. Avilés-García, O.; Espino-Valencia, J.; Mendoza-Zepeda, A.; Donkor, K.; Brewer, S.; Romero, R.; Natividad, R. Removal of metoprolol by means of photo-oxidation processes. *Catal. Today* **2021**, *397–399*, 562–573. [[CrossRef](#)]
39. Bensouici, F.; Bououdina, M.; Dakhel, A.A.; Tala-Ighil, R.; Tounane, M.; Iratni, A.; Souier, T.; Liu, S.; Cai, W. Optical, structural and photocatalysis properties of Cu-doped TiO<sub>2</sub> thin films. *Appl. Surf. Sci.* **2017**, *395*, 110–116. [[CrossRef](#)]
40. Sudrajat, H.; Nguyen, T.K. Key factors controlling the durability of a Cu-doped TiO<sub>2</sub> photocatalyst. *Optik* **2020**, *217*, 164914. [[CrossRef](#)]
41. Avilés-García, O.; Espino-Valencia, J.; Romero, R.; Rico-Cerda, J.L.; Arroyo-Albiter, M.; Natividad, R. W and Mo doped TiO<sub>2</sub>: Synthesis, characterization and photocatalytic activity. *Fuel* **2017**, *198*, 31–41. [[CrossRef](#)]
42. Crişan, M.; Răileanu, M.; Drăgan, N.; Crişan, D.; Ianculescu, A.; Niţoi, I.; Oancea, P.; Şomăcescu, S.; Stănică, N.; Vasile, B.; et al. Sol–gel iron-doped TiO<sub>2</sub> nanopowders with photocatalytic activity. *Appl. Catal. A Gen.* **2015**, *504*, 130–142. [[CrossRef](#)]
43. Avilés-García, O.; Espino-Valencia, J.; Romero-Romero, R.; Rico-Cerda, J.; Arroyo-Albiter, M.; Solís-Casados, D.; Natividad-Rangel, R. Enhanced Photocatalytic Activity of Titania by Co-Doping with Mo and W. *Catalysts* **2018**, *8*, 631. [[CrossRef](#)]
44. Samet, L.; March, K.; Stephan, O.; Brun, N.; Hosni, F.; Bessousa, F.; Benasseur, J.; Chtourou, R. Radiocatalytic Cu-incorporated TiO<sub>2</sub> nano-particles for the degradation of organic species under gamma irradiation. *J. Alloys Compd.* **2018**, *743*, 175–186. [[CrossRef](#)]
45. Zhang, J.; Xu, L.J.; Zhu, Z.Q.; Liu, Q.J. Synthesis and properties of (Yb, N)-TiO<sub>2</sub> photocatalyst for degradation of methylene blue (MB) under visible light irradiation. *Mater. Res. Bull.* **2015**, *70*, 358–364. [[CrossRef](#)]
46. Payormhorm, J.; Idem, R. Synthesis of C-doped TiO<sub>2</sub> by sol-microwave method for photocatalytic conversion of glycerol to value-added chemicals under visible light. *Appl. Catal. A Gen.* **2020**, *590*, 117362. [[CrossRef](#)]
47. Bautista, E.; Ávila-Martínez, E.G.; Natividad, R.; Murcia, J.J.; Romero, R.; Cubillos, J.; Rojas, H.; Hernández, J.S.; Cárdenas, O.; Hidalgo, M.C.; et al. Fluorinated and Platinized Titania for Glycerol Oxidation. *Mater. Proc.* **2021**, *4*, 37. [[CrossRef](#)]
48. Galindo, C.; Jacques, P.; Kalt, A. Photodegradation of the aminoazobenzene acid orange 52 by three advanced oxidation processes: UV/H<sub>2</sub>O<sub>2</sub>, UV/TiO<sub>2</sub> and VIS/TiO<sub>2</sub>: Comparative mechanistic and kinetic investigations. *J. Photochem. Photobiol. A Chem.* **2000**, *130*, 35–47. [[CrossRef](#)]
49. Chekuri, R.D.; Tirukkavalluri, S.R. One step synthesis and characterization of copper doped sulfated titania and its enhanced photocatalytic activity in visible light by degradation of methyl orange. *Chin. J. Chem. Eng.* **2016**, *24*, 475–483. [[CrossRef](#)]
50. Jedsukontorn, T.; Ueno, T.; Saito, N.; Hunsom, M. Mechanistic aspect based on the role of reactive oxidizing species (ROS) in macroscopic level on the glycerol photooxidation over defected and defected-free TiO<sub>2</sub>. *J. Photochem. Photobiol. A Chem.* **2018**, *367*, 270–281. [[CrossRef](#)]
51. Mendoza, A.; Romero, R.; Gutiérrez-Cedillo, G.P.; López-Tellez, G.; Lorenzo-González, O.; Gómez-Espinosa, R.M.; Natividad, R. Selective production of dihydroxyacetone and glyceraldehyde by photo-assisted oxidation of glycerol. *Catal. Today* **2020**, *358*, 149–154. [[CrossRef](#)]
52. Hu, W.; Knight, D.; Lowry, B.; Varma, A. Selective Oxidation of Glycerol to Dihydroxyacetone over Pt–Bi/C Catalyst: Optimization of Catalyst and Reaction Conditions. *Ind. Eng. Chem. Res.* **2010**, *49*, 10876–10882. [[CrossRef](#)]
53. Gil, S.; Marchena, M.; Sánchez-Silva, L.; Romero, A.; Sánchez, P.; Valverde, J.L. Effect of the operation conditions on the selective oxidation of glycerol with catalysts based on Au supported on carbonaceous materials. *Chem. Eng. J.* **2011**, *178*, 423–435. [[CrossRef](#)]
54. Oliveira, V.L.; Morais, C.; Servat, K.; Napporn, T.W.; Olivi, P.; Kokoh, K.B.; Tremiliosi-Filho, G. Kinetic Investigations of Glycerol Oxidation Reaction on Ni/C. *Electrocatalysis* **2015**, *6*, 447–454. [[CrossRef](#)]
55. Wu, G.; Liu, Y.; He, Y.; Feng, J.; Li, D. Reaction pathway investigation using in situ Fourier transform infrared technique over Pt/CuO and Pt/TiO<sub>2</sub> for selective glycerol oxidation. *Appl. Catal. B Environ.* **2021**, *291*, 120061. [[CrossRef](#)]
56. Jensen, W.A. Response Surface Methodology: Process and Product Optimization Using Designed Experiments. In *Journal of Quality Technology*, 4th ed.; Taylor & Francis: Oxfordshire, UK, 2017; Volume 49, pp. 186–188. [[CrossRef](#)]
57. Augugliaro, V.; El Nazer, H.A.H.; Loddo, V.; Mele, A.; Palmisano, G.; Palmisano, L.; Yurdakal, S. Partial photocatalytic oxidation of glycerol in TiO<sub>2</sub> water suspensions. *Catal. Today* **2010**, *151*, 21–28. [[CrossRef](#)]
58. Yu, J.; Dappozze, F.; Martín-Gomez, J.; Hidalgo-Carrillo, J.; Marinas, A.; Vernoux, P.; Cravana, A.; Guillard, C. Glyceraldehyde production by photocatalytic oxidation of glycerol on WO<sub>3</sub>-based materials. *Appl. Catal. B Environ.* **2021**, *299*, 120616. [[CrossRef](#)]

59. Hurtado, L.; Avilés, O.; Brewer, S.; Donkor, K.K.; Romero, R.; Gómez-Espinosa, R.M.; Alvarado, O.; Natividad, R. Al/Cu-PILC as a Photo-Fenton Catalyst: Paracetamol Mineralization. *ACS Omega* **2022**, *7*, 23821–23832. [[CrossRef](#)] [[PubMed](#)]
60. Wang, J.; Cherevan, A.S.; Hannecart, C.; Naghdi, S.; Nandan, S.P.; Gupta, T.; Eder, D. Ti-based MOFs: New insights on the impact of ligand composition and hole scavengers on stability, charge separation and photocatalytic hydrogen evolution. *Appl. Catal. B Environ.* **2021**, *283*, 119626. [[CrossRef](#)]
61. Wei, Y.; Cheng, G.; Xiong, J.; Zhu, J.; Gan, Y.; Zhang, M.; Li, Z.; Dou, S. Synergistic impact of cocatalysts and hole scavenger for promoted photocatalytic H<sub>2</sub> evolution in mesoporous TiO<sub>2</sub>NiS<sub>x</sub> hybrid. *J. Energy Chem.* **2019**, *32*, 45–56. [[CrossRef](#)]
62. Peralta, E.; Roa, G.; Hernandez-Servin, J.A.; Romero, R.; Balderas, P.; Natividad, R. Hydroxyl Radicals quantification by UV spectrophotometry. *Electrochim. Acta* **2014**, *129*, 137–141. [[CrossRef](#)]
63. Alvarado-Rolon, O.; Natividad, R.; Ramírez-García, J.; Orozco-Velazco, J.; Hernandez-Servin, J.A.; Ramírez-Serrano, A. Kinetic modelling of paracetamol degradation by photocatalysis: Incorporating the competition for photons by the organic molecule and the photocatalyst. *J. Photochem. Photobiol. A Chem.* **2021**, *412*, 113252. [[CrossRef](#)]